Monthly Notices
of the
ROYAL ASTRONOMICAL SOCIETY

MNRAS 458, 3561–3577 (2016)
Advance Access publication 2016 March 8

doi:10.1093/mnras/stw553

Non-radial pulsation in first overtone Cepheids of the Small Magellanic Cloud

R. Smolec[1]★ and M. Śniegowska[2]

[1]*Nicolaus Copernicus Astronomical Center, Polish Academy of Sciences, ul. Bartycka 18, PL-00-716 Warszawa, Poland*
[2]*Warsaw University Observatory, Al. Ujazdowskie 4, PL-00-478 Warszawa, Poland*

Accepted 2016 March 3. Received 2016 March 3; in original form 2015 December 23

ABSTRACT

We analyse photometry for 138 first overtone Cepheids from the Small Magellanic Cloud, in which Optical Gravitational Lensing Experiment team discovered additional variability with period shorter than first overtone period, and period ratios in the $P/P_{1O} \in (0.60, 0.65)$ range. In the Petersen diagram, these stars form three well-separated sequences. The additional variability cannot correspond to other radial mode. This form of pulsation is still puzzling. We find that amplitude of the additional variability is small, typically 2–4 per cent of the first overtone amplitude, which corresponds to 2–5 mmag. In some stars, we find simultaneously two close periodicities corresponding to two sequences in the Petersen diagram. The most important finding is the detection of power excess at half the frequency of the additional variability (at subharmonic) in 35 per cent of the analysed stars. Interestingly, power excess at subharmonic frequency is detected mostly for stars of the middle sequence in the Petersen diagram (74 per cent), incidence rate is much lower for stars of the top sequence (31 per cent), and phenomenon is not detected for stars of the bottom sequence. The amplitude and/or phase of the additional periodicities strongly vary in time. Similar form of pulsation is observed in first overtone RR Lyrae stars. Our results indicate that the nature and cause of this form of pulsation is the same in the two groups of classical pulsators; consequently, a common model explaining this form of pulsation should be searched for. Our results favour the theory of the excitation of non-radial modes of angular degrees 7, 8 and 9, proposed recently by Dziembowski.

Key words: methods: data analysis – stars: oscillations – stars: variables: Cepheids – Magellanic Clouds.

1 INTRODUCTION

The majority of classical Cepheids are single-periodic, radial pulsators. More complex pulsation is not rare, however. Double-mode Cepheids pulsating simultaneously in the radial fundamental and in the radial first overtone modes (F+1O) and in the two lowest order radial overtones (1O+2O) are known for years. These form of pulsation is recognized based on characteristic period ratios of the excited pulsation modes, $P_{2O}/P_{1O} \approx 0.80$–$0.81$ for 1O+2O pulsators and $P_{1O}/P_F \approx 0.715$–0.74 for F+1O pulsators (e.g. Soszyński et al. 2008b, 2010). A well-known fact is that period ratio depends on metallicity; characteristic values may slightly differ for stars from different stellar systems. The Optical Gravitational Lensing Experiment (OGLE; Udalski et al. 2008; Udalski, Szymański & Szymański 2015) observations led to the discovery of other forms of multiperiodic pulsation among Cepheids. Triple-mode radial pulsation, F+1O+2O and 1O+2O+3O, was identified (Moskalik, Kołaczkowski & Mizerski 2004; Soszyński et al. 2008a, 2010, 2011, 2015). A very interesting triple-mode Cepheid, with 1O, 2O and additional longer period mode, was discovered with *CoRoT* (Poretti, Baglin & Weiss 2014). Rare and peculiar double-mode pulsations were also discovered, including 1O+3O pulsation with 2O apparently not excited (Soszyński et al. 2008a, 2015) and first double-mode 2O+3O Cepheid (Soszyński et al. 2015). For recent review, see Moskalik (2014).

The analysis of 1O Cepheids revealed another, most interesting group of double-periodic pulsators. In more than hundred 1O Cepheids additional small-amplitude variability, with period shorter than first overtone period, was detected. The period ratios fall in the $P/P_{1O} \in (0.6, 0.65)$ range and cannot correspond to two radial modes (Dziembowski & Smolec 2009). 35 stars were reported in the Large Magellanic Cloud (LMC; Soszyński et al. 2008b; Moskalik & Kołaczkowski 2009), 138 stars in the Small Magellanic Cloud (SMC; Soszyński et al. 2010) and 1 star was found in the Galactic disc (Pietrukowicz et al. 2013). One LMC star with additional

★ E-mail: smolec@camk.edu.pl

variability pulsates simultaneously in the radial fundamental and first overtone modes (Moskalik & Kołaczkowski 2009). Two stars were also identified in the *Kepler-K2* photometry (Plachy et al., in preparation). In the Petersen diagram, i.e. in the plot of shorter-to-longer period ratio versus the longer period, these stars group in the three well separated sequences.

Interestingly, very similar form of pulsation is present in RR Lyrae stars, see the most in-depth and extensive studies of the phenomenon by Moskalik et al. (2015), Netzel, Smolec & Moskalik (2015a,b) and Jurcsik et al. (2015). Additional variability is detected in first overtone pulsators (RRc) or in double-mode F+1O pulsators (RRd). Period ratios fall in the similar range, $P/P_{1O} \in (0.60, 0.64)$. Three sequences are present in the Petersen diagram as well, although they are not that well separated as in the case of Cepheids (Netzel et al. 2015b). Thanks to ultra-precise observations by space telescopes, *Kepler* and *CoRoT* (e.g. Szabó, Benkő & Paparó 2014; Molnár et al. 2015; Moskalik et al. 2015; Kurtz et al. 2016), and detailed analysis of ground-based observations (Netzel et al. 2015a,b; Jurcsik et al. 2015) this form of pulsation is well studied in RR Lyr stars. In particular, we know that in the frequency spectra of these stars, signal (power excess) at subharmonic of the additional frequency is present. Signals associated with the additional variability are broad and non-coherent. In the time domain, it corresponds to strong variability of amplitude and frequency on a time-scale of a few tens to hundreds of days. The phenomenon must be common among RRc/RRd stars, as 14 out of 15 stars observed from space show this form of pulsation (for a summary, see Moskalik et al. 2015).

In contrast to RR Lyr stars, 1O Cepheids were not extensively observed from space (see Section 4.1). Analysis of ground-based data, in particular of the largest sample of 138 of these interesting stars from SMC is missing. Soszyński et al. (2010) only reported the discovery of these stars and provided their periods and period ratios. In the present study, we analyse the OGLE-III data for these interesting objects in detail. We do not search for additional objects, but focus on those in which we know that additional variability is present. Our goal is to study the properties of the variability in detail. In particular, we check for the presence of subharmonics of the additional signal, analyse the amplitude distribution and time-variation of the additional signals. These are necessary information for the models and theories to explain this peculiar and puzzling form of pulsation.

2 DATA ANALYSIS

We analyse OGLE-III *I*-band photometry for 138 stars listed in Soszyński et al. (2010). All these stars were identified as 1O Cepheids with additional small amplitude variability, with period ratios in the $P/P_{1O} \in (0.6, 0.65)$ range. We use standard consecutive pre-whitening technique. We identify the dominant frequencies with the help of discrete Fourier transform (FT). Next, we fit the data with the sine series of the following form:

$$m(t) = m_0 + \sum_k A_k \sin(2\pi \nu_k t + \phi_k), \quad (1)$$

using the non-linear least-square fitting. The FT of residual data is inspected for the presence of additional signals, which are iteratively included in equation (1). Only resolved frequencies are included. We consider two peaks as well resolved if their separation is larger than $2/\Delta T$, where ΔT is data length. In the FT, the signal is considered significant if signal-to-noise ratio (S/N) exceeds 4. The criterion is relaxed for signals at combination frequencies, provided that peak is present exactly (within frequency resolution) at the expected position (we accept S/N > 3.5). Typically our solution consists of low-order (3–6) Fourier series describing the dominant variability associated with the first overtone ($k\nu_{1O}$), sine term with the frequency of the additional variability of interest (ν_x) and possibly with the combination frequency with the first overtone frequency (typically $\nu_{1O} + \nu_x$). Additional significant signals we find, that do not fall in the $P/P_{1O} \in (0.6, 0.65)$ range, are also included in equation (1).

During the analysis we reject the outliers (4σ criterion) and remove slow trends through subtracting from the original data the low-order polynomials or splines. These functions are fitted to the residuals. Quite often, after pre-whitening with the first overtone frequency and its harmonics, residual signal remains at the location unresolved with $k\nu_{1O}$. Typically it corresponds to the long-term variation of the first overtone phase (period change). This signal may be significant which increases the noise level in the FT and consequently may hide the additional variabilities. In such case, we get rid of the non-stationary first overtone variation with the help of time-dependent pre-whitening technique, described and applied to the *Kepler* data by Moskalik et al. (2015). Application to the ground-based OGLE data is described in more detail in Netzel et al. (2015a).

Strong daily aliases and 1-yr aliases are inherent to ground-based OGLE observations of the SMC. As the signals we search for are relatively weak, the alias-related ambiguities can happen. In some stars, after pre-whitening with the first overtone frequency, we detect a few significant peaks of similar height which are mutual daily aliases. If period corresponding to one of them falls in the $P/P_{1O} \in (0.6, 0.65)$ range, then this peak is accepted as a true signal, even if it is not the highest peak. All such cases are reported explicitly in the study.

3 RESULTS

3.1 Overview

Results of our analysis are collected in Table A1 in the Appendix. For a reference, a section of the Table is presented in Table 1. In consecutive columns there are: star's id, first overtone period, P_{1O}, period of the additional variability in the $P/P_{1O} \in (0.6, 0.65)$ range, P_x, period ratio, P_x/P_{1O}, amplitude of the first overtone mode, amplitude ratio, A_x/A_{1O}, and remarks. The resulting Petersen diagram is plotted in Fig. 1.

In the frequency spectrum, the additional variability rarely appears as a single and coherent peak. Typically more complex structures are present; examples are illustrated in Fig. 2. Sometimes two dominant close peaks are detected, as illustrated in the top two panels of Fig. 2. In other cases the signal appears as a complex cluster of peaks, as illustrated in the two lower panels of Fig. 2. In our analysis, we pick the highest peak in the cluster, or in a group of close peaks (marked with filled diamonds in Fig. 2), and include its frequency in equation (1). Its properties, period and amplitude, P_x and A_x, are then given in Table 1. After pre-whitening, residual, unresolved power is often detected. Such appearance of additional variability indicates that it is strongly non-stationary, with variable phase and/or amplitude (see Section 3.6). All stars in which more complex structures are detected at ν_x (two close peaks, clusters of peaks, residual power after pre-whitening) are marked with 'nsx' in the remarks column of Table 1. These structures indicate that additional variability is non-stationary, see Section 3.6. The different appearance of the signal may result from different time-scales of

Table 1. Properties of 1O Cepheids with additional variability. The consecutive columns contain: star's id, first overtone period, P_{1O}, period of the additional variability, P_x, period ratio, P_x/P_{1O}, amplitude of the first overtone, A_{1O}, and amplitude ratio, A_x/A_{1O}, and remarks: 'al' – daily alias of signal at ν_x is higher; 'nsx' – complex appearance of the signal at ν_x; 'nsO' – non-stationary first overtone; 'cf' – combination frequency of ν_x and ν_{1O} detected; 'sh' – power excess at subharmonic frequency (centred at $1/2\nu_x$) detected; 'ap' – additional periodicity detected; 'tdp' – time-dependent analysis was conducted; '?' – weak detection (S/N given in the parenthesis). Full table is in the Appendix A (Table A1).

Star	P_{1O} (d)	P_x (d)	P_x/P_{1O}	A_{1O} (mag)	A_x/A_{1O}	Remarks
OGLE-SMC-CEP-0056	0.9860208(7)	0.60373(1)	0.6123	0.1689	0.024	? (S/N = 3.77)
OGLE-SMC-CEP-0212	1.741010(4)	1.08766(4)	0.6247	0.0997	0.036	sh, nsx
OGLE-SMC-CEP-0251	1.796802(1)	1.12279(2)	0.6249	0.1399	0.029	sh, nsx
OGLE-SMC-CEP-0280	1.675191(1)	1.04344(2)	0.6229	0.1377	0.026	nsO, ap
OGLE-SMC-CEP-0281	1.2662457(7)	0.774075(9)	0.6113	0.1263	0.033	al, nsx
OGLE-SMC-CEP-0307	0.9734743(7)	0.59718(1)	0.6134	0.1922	0.019	nsO, ap
OGLE-SMC-CEP-0447	1.2651448(8)	0.77624(1)	0.6136	0.1300	0.024	nsO, nsx
...						

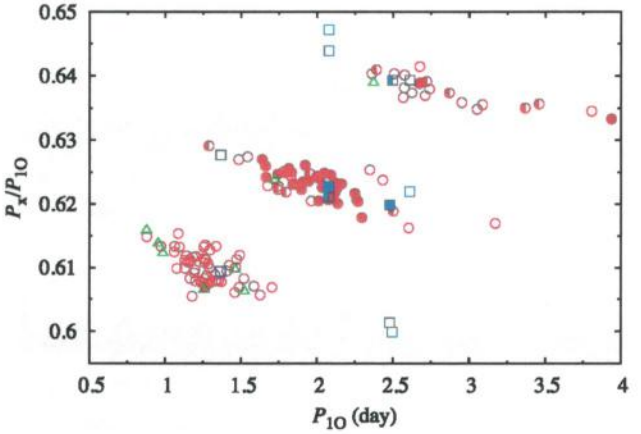

Figure 1. Petersen diagram for 138 analysed Cepheids. Stars in which two periodicities were detected, corresponding to two sequences in the diagram, are marked with squares (two squares per star). Stars with weak detection of the additional periodicity are marked with open triangles. Filled symbols correspond to stars in which power excess centred at subharmonic frequency, $\nu_x/2$, was detected (half-filled symbols are used to indicate weak detections).

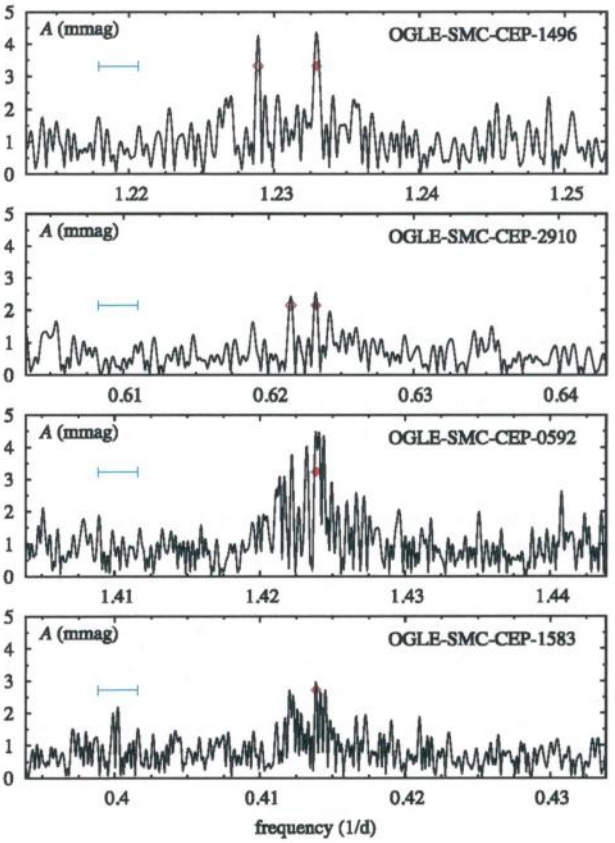

Figure 2. Illustration of complex structures detected at ν_x. In the two upper panels, two well-separated peaks of similar height are present, while in the two lower panels, clusters of peaks are present. The extent of the horizontal bar corresponds to the separation expected for 1-yr alias. Filled diamonds mark the location of peaks included in Table 1. In the two upper panels, open diamonds indicate the location of peaks adopted by Soszyński et al. (2010) (see Appendix, Section B).

the variability and different structure of the data (different length of the available data). There are 80 stars marked with 'nsx' which is 58 per cent of the analysed sample. The complex structures at ν_x are common.

First overtone is often non-stationary as well, which appears as strong unresolved power at its frequency, after the pre-whitening. These stars are marked with 'nsO' in Table 1. There are 56 such stars which constitutes nearly 41 per cent of the analysed sample. In some cases, the unresolved power at ν_{1O} dominates the frequency spectrum and significantly increases the noise level in the FT, which may hide the additional significant peaks. In all such cases, we conducted time-dependent pre-whitening to get rid of the unwanted signal. If time-dependent pre-whitening was crucial for the detection of additional variability of interest, or significantly improved the S/N of the interesting peak at ν_x, then 'tdp' is included in the remarks column of Table 1. In these cases, the frequency and amplitude of the additional variability are determined independently of the determination of amplitude and frequency of the first overtone, from the data set with first overtone filtered out. An inherent part of the time-dependent pre-whitening is time-dependent Fourier analysis, which shows how the amplitude and phase of the first overtone change in time. In the majority of cases, we observed a pronounced phase change, while amplitude changes were insignificant. No firm case of Blazhko-like modulation was found, although in some cases variation of first overtone phase seemed periodic.

Fast period changes, on time-scale shorter than expected from evolutionary calculations are common in 1O Cepheids. Exemplary O-C diagrams may be found e.g. in studies by Berdnikov & Pastukhova (1994) or Berdnikov et al. (1997). A detailed study of OGLE and MACHO data for LMC Cepheids was conducted by Poleski (2008) who detected period changes in 41 per cent of 1O LMC Cepheids and in 18 per cent of fundamental mode pulsators.

The analysis of period changes of the first overtone is beyond the scope of the present analysis; however, dedicated study is planned.

In 25 stars, we find peaks at combination frequency, $\nu_{1O} + \nu_x$, and in one star we find peak at $\nu_x - \nu_{1O}$ (OGLE-SMC-CEP-0797). These stars are marked with 'cf' in the last column of Table 1.

Stars in which signal at a daily alias of ν_x is higher are marked with 'al'. As described in the previous section, we select the lower alias as a true signal if it falls well within one of the three sequences in the Petersen diagram.

In 17 stars marked with 'ap' in Table 1, we detect additional significant periodicity that does not fall into the $P/P_{1O} \in (0.60, 0.65)$ range and cannot be interpreted as due to other radial mode. In a few stars, the additional peaks appear relatively close to the radial first overtone frequency. We note that similar detections were reported by Moskalik & Kołaczkowski (2009), who argue that these signals may be intrinsic to the stars and correspond to non-radial pulsation. In no case we detect combination frequency with the first overtone, however. In principle, these periodicities may result from blending. We postpone the discussion of these additional signals till the analysis of full sample of SMC Cepheids, which will allow us to draw some statistically meaningful conclusions concerning their nature.

In stars plotted with triangle in Fig. 1, the detection of additional variability is weak. These stars are marked with '?' and S/N value is given in the last column of Table 1. In some cases, the additional signal appeared only after the time-dependent pre-whitening. There are eight such cases and we discuss them in more detail in the Appendix, in Section B, which also contains detailed comparison of our results with those reported in Soszyński et al. (2010). The period ratios for these stars fall well within the three sequences in the Petersen diagram. Despite the weak detection, we consider these stars as double-periodic in the following.

In six stars, two well separated and significant peaks were detected in the frequency range of interest – the corresponding period ratios fall within two separate sequences in Fig. 1. In the figure, these stars are marked with squares, two for each of six stars. Their frequency spectra are plotted in Fig. 3. Typically, signal corresponding to one of the sequences is dominant, while the detection of peak corresponding to the other sequence is rather weak (but always with S/N > 4.0). In Table 1, two rows are present for these stars, with characteristics of the highest peaks falling within one of the sequences. All other stars, in which we detect a significant peak corresponding to only one sequence, are marked with circles in Fig. 1.

Finally, in many stars we detect significant power centred at $1/2\nu_x$, i.e. at subharmonic frequency. These stars are marked with 'sh' in the remarks column of Table 1, printed in italics if the detection is weak. In the Petersen diagram in Fig. 1, stars with firm detection of the power excess at subharmonic frequency are marked with filled symbols. In the case of weak detection, half-filled symbol is plotted. These signals will be discussed in detail in Section 3.4.

3.2 The Petersen diagram and amplitude distributions

Three well separated and slanted sequences are present in the Petersen diagram (Fig. 1). 64 stars fall within the bottom sequence, 54 stars fall within the middle sequence and 26 stars fall within the top sequence. The numbers do not add up to 138, as six stars fall within two sequences simultaneously. Within each sequence, period ratio drops with the increasing pulsation period. Stars forming the bottom sequence have, on average, shorter pulsation periods, while stars forming the top sequence have, on average, longer pulsation periods.

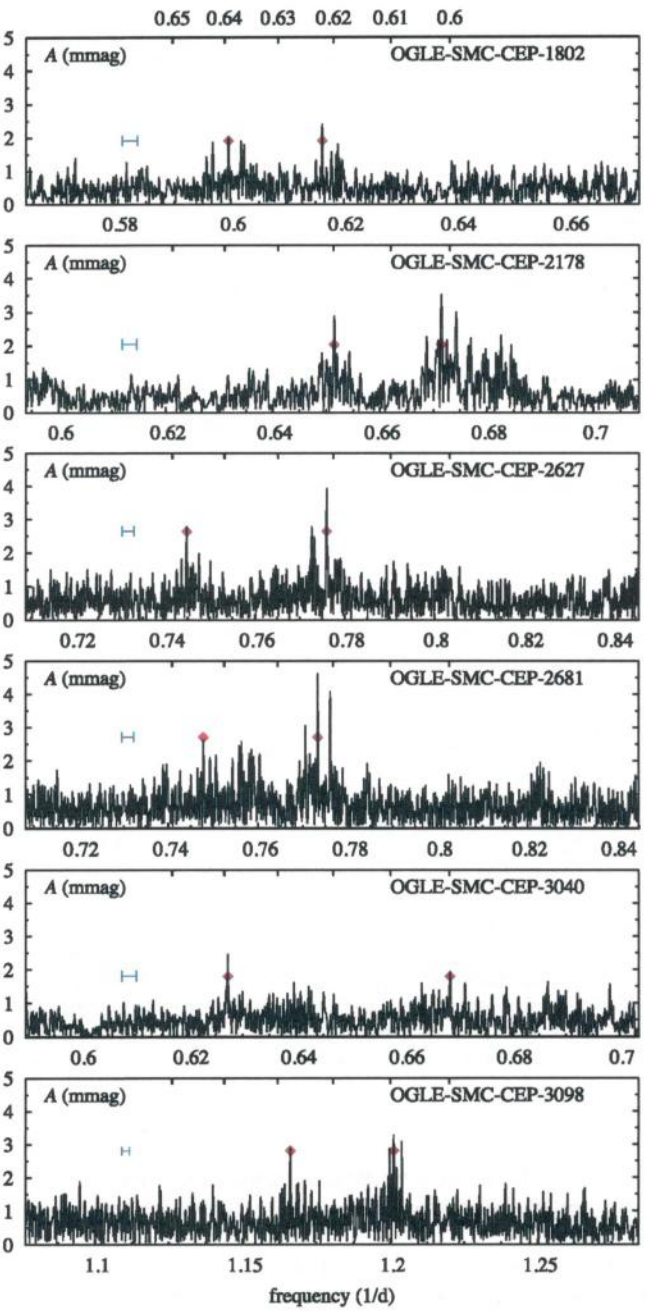

Figure 3. Frequency spectra for six stars in which two significant peaks, corresponding to two sequences in the Petersen diagram, were detected. These peaks are marked with filled diamonds placed at the S/N = 4.0 level. The extent of the horizontal bar, plotted in each panel, corresponds to separation expected for 1-yr aliases. Period-ratio scale, P/P_{1O}, is plotted at the top of each panel, with numerical labels plotted in the top-most panel.

The number of stars in the top sequence is significantly smaller than in the middle and bottom sequences. On the other hand, long-period first overtone Cepheids are not as numerous as short-period overtone pulsators. In Fig. 4, we study the period distribution for all 1644 first overtone SMC Cepheids from OGLE-III collection (solid black line) and for stars with additional variability (hatched area; three different patterns show the contributions from the three sequences). Stars were counted in 0.5 d-wide bins, except $P_{1O} <$ 1 d, where we used smaller, 0.25 d-wide bins. This is because of sharp increase of Cepheid number as one moves from 0.25–0.5 d

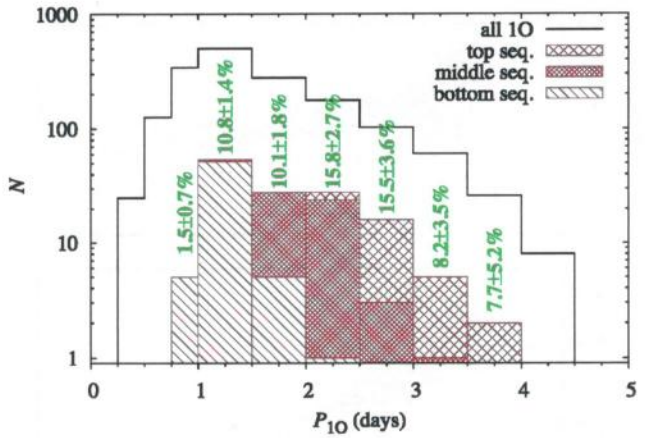

Figure 4. Period distribution for all 1O SMC OGLE-III Cepheids (solid black line) and for stars with the additional variability (hatched area). Contributions from the three sequences in the Petersen diagram are marked with different patterns, as indicated in the key. Incidence rates are also provided.

bin through 0.5–0.75 d bin to 0.75–1.0 d bin. Within each bin the incidence rate of stars with additional variability is given with statistical errors calculated assuming that the population follows a Poisson distribution (e.g. Alcock et al. 2003).

It is well visible that the discussed form of pulsation is not present in the shortest period 1O Cepheids with $P_{1O} < 0.75$ d, despite of 151 stars falling into this period range. For $0.75\,\mathrm{d} < P_{1O} < 1.0\,\mathrm{d}$, there are 342 1O Cepheids and only in five of them the additional variability was found. Incidence rate is very low (1.5 ± 0.7 per cent) as compared to the next longer-period bin (10.8 ± 1.4 per cent). This is most likely due to selection effect. Shortest period overtone Cepheids are least luminous (because of the P–L relation, see Fig. 7), consequently one may expect higher noise level in the FT, which may hinder the detection of low-amplitude variability. This is discussed in more detail in Section 3.5. For $P_{1O} > 1$ d, the discussed form of pulsation is quite frequent. For $1\,\mathrm{d} \leq P_{1O} < 2\mathrm{d}$, the incidence rate is ≈10.5 per cent, for $2\,\mathrm{d} \leq P_{1O} < 3\,\mathrm{d}$, it is ≈15.5 per cent, and for $3\,\mathrm{d} \leq P_{1O} < 4\,\mathrm{d}$, it is ≈8 per cent. Taking into account the statistical errors, these numbers are not that different. We conclude that the top sequence is the least numerous of the three, mostly because there are fewer long-period 1O Cepheids than short-period ones and also because the incidence rate may be slightly lower for longer periods.

The additional variability is always weak as compared to radial first overtone. Table 1 provides the amplitude of the first overtone, A_{1O}, and amplitude ratio, A_x/A_{1O}. The top panel of Fig. 5 shows the amplitude of the first overtone as a function of the first overtone period. The amplitude drops with increasing pulsation period. The highest (Fourier) amplitude is slightly below 0.2 mag, the lowest is around 0.06 mag. The most typical values fall in the 0.10–0.16 mag range. In the middle panel of Fig. 5, we plot the amplitude of the first overtone as a function of period ratio, P_x/P_{1O}. The trace of the three sequences present in the Petersen diagram is well visible. It is clear that amplitudes are the highest in stars forming the bottom sequence (as these stars have shorter first overtone periods, on average) and the lowest in the stars forming the top sequence (stars with longer first overtone periods). The bottom panel of Fig. 5 shows the amplitude ratio, A_x/A_{1O}, as a function of period ratio. There is no significant difference between the stars corresponding to the three sequences. In stars that are plotted with filled symbols in Fig. 5, a power excess at subharmonic, $1/2\nu_x$, is detected. This will be

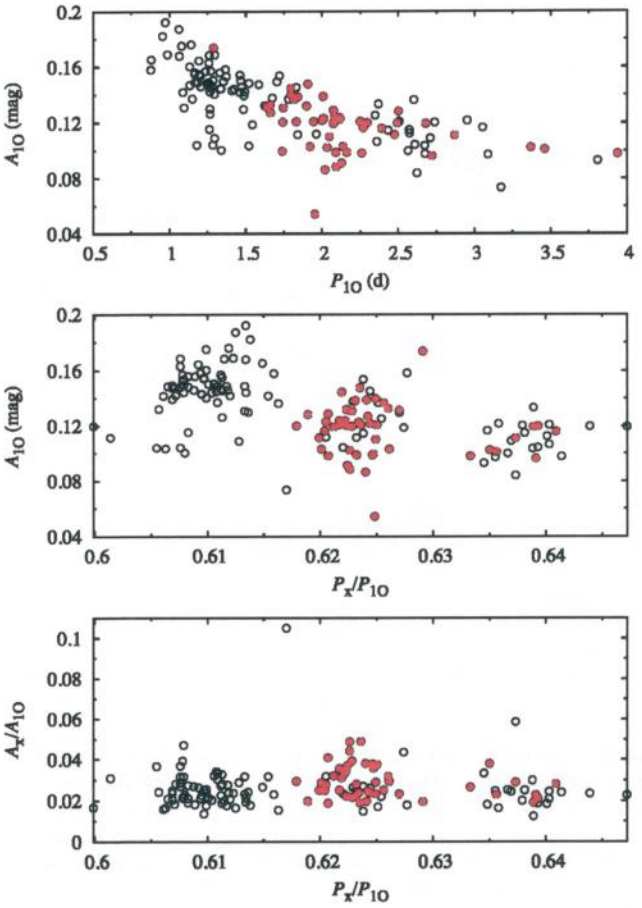

Figure 5. First overtone amplitude as a function of P_{1O} (top panel) and P_x/P_{1O} (middle panel). In the bottom panel, we show A_x/A_{1O} as a function of P_x/P_{1O}. Stars in which power excess at subharmonic, $1/2\nu_x$, was detected are plotted with filled symbols.

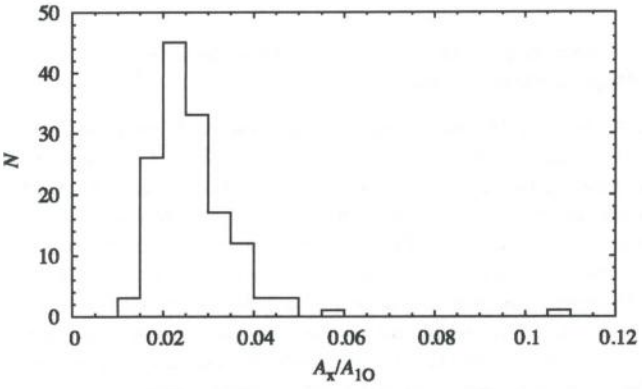

Figure 6. Histogram of A_x/A_{1O} values.

discussed in more detail in Section 3.4. Here we just note that for stars of the middle and top sequences (only there power excess at subharmonic was detected) there is no difference in first overtone amplitude between stars with, and stars without power excess at subharmonic. The histogram of amplitude ratios, A_x/A_{1O}, for all the stars is presented in Fig. 6. The distribution peaks at A_x/A_{1O} ≈ 1.75–2.25 per cent. Typical amplitudes of the additional variability are in the 2–5 mmag range (see also Fig. 12). It explains why the additional variability was discovered only recently – high-quality observations are necessary to detect such low-amplitude

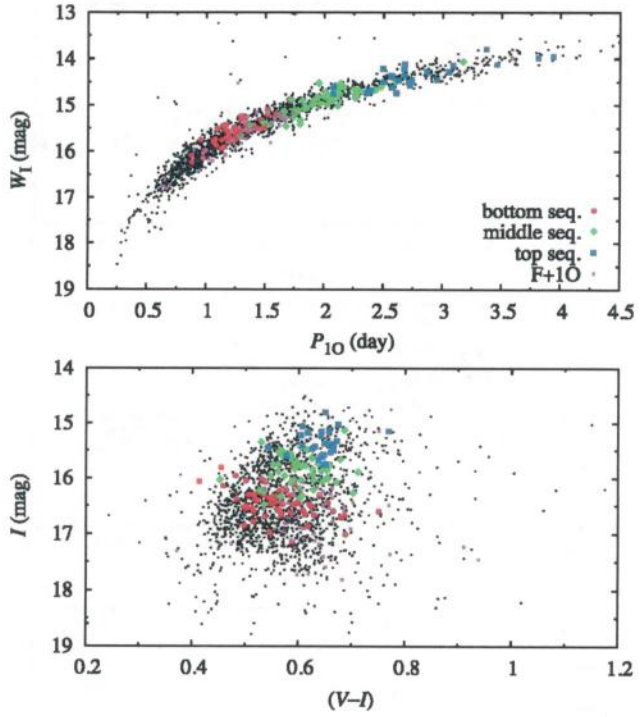

Figure 7. Period–luminosity (top panel) and colour–magnitude (bottom panel) diagrams for all 1O Cepheids from the SMC OGLE-III collection (small dots) and for Cepheids with additional variability analysed in this paper (larger symbols; red circles correspond to the bottom sequence in the Petersen diagram, green diamonds to the middle sequence and blue squares to the top sequence). In addition, double-mode, F+1O Cepheids are plotted with small squares.

variability. So far, the signal was detected mostly in the excellent OGLE data. Additional variability was also detected in two 1O Cepheids observed with *K2* (Plachy et al., in preparation).

3.3 Comparison with other first overtone Cepheids without additional variability

In this section, we check whether Cepheids with additional variability differ significantly from other first overtone SMC Cepheids, that are single-periodic. In Fig. 7, we plot the location of analysed stars in the period–luminosity (top panel) and in the colour–magnitude (bottom panel) diagrams. For the former diagram, we use reddening free Wesenheit index as the luminosity indicator. In the plots, all 1O Cepheids are plotted with small black dots, while stars with additional variability are plotted with larger symbols; point shape and point colour code the star's location in the Petersen diagram (red circles – bottom sequence, green diamonds – middle sequence and blue squares – top sequence). Stars in which variability corresponding to two sequences was detected, are plotted only once, as members of the sequence for which corresponding amplitude is higher. For this plot, periods and intensity mean *I*- and *V*-band magnitudes were taken directly from the OGLE-III ftp archive (Soszyński et al. 2010).

Except the lack of additional variability in the shortest period stars ($P_{1O} < 0.8$ d), which we already noted in the previous section, we see no significant differences in the distribution of stars with and without the additional variability in the two diagrams presented in Fig. 7. They cover similar colour and Wesenheit index ranges. Separation of stars, members of the three sequences in the Petersen diagram,

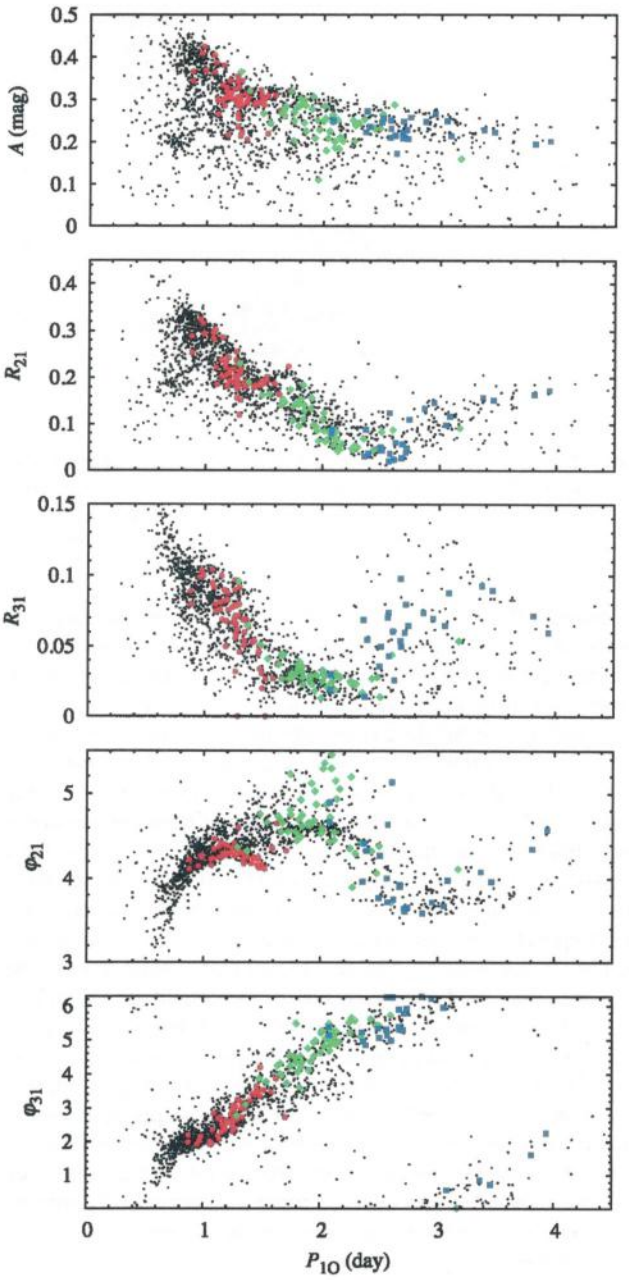

Figure 8. Fourier decomposition parameters versus the first overtone period for all 1O Cepheids from the SMC OGLE-III collection (small dots) and for Cepheids with additional variability analysed in this paper (larger symbols, as in Fig. 7).

is clear and pronounced. As period–luminosity diagram indicates, it results from different first overtone periods characteristic for the three groups. Members of the bottom sequence have shorter periods and consequently are least luminous, while members of the top sequence have longer periods and are thus most luminous. For stars of each sequence the covered colour range is similar as for single-periodic stars of similar luminosity. In Fig. 7, we also plotted double-mode F+1O Cepheids (small squares). These stars cover similar luminosity range as stars of the bottom sequence, but are shifted, on average, towards higher colour values.

In Fig. 8, we compare the light-curve shapes with the help of the Fourier decomposition parameters (Simon & Lee 1981). Symbols used in the panels are exactly the same as in Fig. 7. In the consecutive

panels, from top to bottom, we plot: peak-to-peak amplitude, R_{21}, R_{31}, φ_{21} and φ_{31}, all as a function of first overtone period. A lack of short period Cepheids with additional variability is again apparent. Also, additional variability is not detected in stars with low first overtone amplitude, $A \lesssim 0.2$ mag (and consequently in stars with lower R_{21} and R_{31}), which is a selection effect. First, these stars are not as numerous as higher amplitude Cepheids. Secondly, with typical amplitude of the additional variability corresponding to ~2–4 per cent of the first overtone amplitude, possible signals are also of lower amplitude and likely hidden in the noise. Otherwise, it seems that Cepheids with additional variability follow the same progressions as Cepheids without additional variability. The only exception seems the behaviour of φ_{21} in the narrow period range of 1.4–1.6 d. In this period bin, 1O Cepheids cover the $4 \lesssim \varphi_{21} \lesssim 5$ range, but stars with additional variability and of the bottom sequence (red circles) prefer the low values, $\varphi_{21} \lesssim 4.3$.

We conclude that there is no significant difference between 1O Cepheids with and without the additional variability, with regards to their location on the period–luminosity and colour–magnitude diagrams, and light-curve shapes (with the possible exception of φ_{21} in relatively narrow period range).

3.4 Subharmonics

In many stars, we detect significant signal centred at $1/2\nu_x$, i.e. at subharmonic of ν_x. Typically, the signal detected at $1/2\nu_x$ has a complex form – broad cluster of peaks, centred at $1/2\nu_x$ is detected. Stars in which such power excess was detected are marked with 'sh' in Table 1. The weak detection is marked with '*sh*'. What we regard as 'weak' is somewhat subjective. In general, if $3.5 < \mathrm{S/N} < 4.0$ for the highest peak at around $1/2\nu_x$, or the power excess was evident only after the time-dependent pre-whitening, the star is marked as a weak detection. In all cases however, the power excess was clear. Altogether, it was detected in 48 stars, of which 14 are marked as weak detections. This constitutes 35 per cent of the analysed sample or, if weak detections are excluded, 25 per cent. Detailed characterization of frequency spectra of stars with power excess detected at subharmonic frequency is collected in Table 2. Power excess is characterized by the frequency and amplitude of the highest peak detected at around $1/2\nu_x$, ν_{sh} and A_{sh}, respectively. Table contains: star's id, period ratio, P_x/P_{1O}, frequency of the additional variability, ν_x, frequency of the highest peak detected around $1/2\nu_x$, ν_{sh}, frequency ratio, ν_{sh}/ν_x, amplitude of the additional variability, A_x, and amplitude ratio, A_{sh}/A_x, approximate S/N for the peak at ν_{sh} and remarks: 'weak' – weak detection, 'broad' – broad power excess; 'tdp' – time-dependent pre-whitening of all signals except ν_{sh} conducted.

No firm detection of power excess at other subharmonic frequencies, i.e. at $3/2\nu_x$, $5/2\nu_x$, etc., is reported. There are a few ambiguous cases, in which power excess is present at $3/2\nu_x$, but sometimes it is an alias of power excess at $1/2\nu_x$ or of unresolved residual power at first overtone frequency. Time-dependent pre-whitening will not help here; by removing e.g. the non-stationary variation at ν_{1O} we also remove the power at its daily aliases.

Before we discuss the properties of the signals detected at subharmonic frequencies, in Figs 9, 10 and 11, we show some examples of structures detected in the frequency spectra of the stars at ν_x and at $1/2\nu_x$. In Fig. 9, we show the cases in which signal at $1/2\nu_x$ is firmly detected and is relatively narrow. In Fig. 10, we show some of the cases in which the signal at $1/2\nu_x$ is broad. Finally, in Fig. 11, we show some cases in which detection of the power excess is weak. Structure of these three figures is the same. For each star, two panels are plotted. In the top panel, the frequency spectrum centred at ν_x is plotted, while in the bottom panel the frequency spectrum centred at $1/2\nu_x$ is plotted. The plotted frequency range is the same in the two panels; it is wider in Figs 10 and 11 for better visualization of the signal at $1/2\nu_x$.

Based on the content of Table 2 and on Figs 9, 10 and 11, we now discuss the properties of the signal detected at $1/2\nu_x$. We first note that the detected power excess is indeed well centred at $1/2\nu_x$. The mean value of ν_{sh}/ν_x for all the stars is 0.5003 ± 0.0010; values of $\nu_{sh}/\nu_x < 0.5$ are as common as $\nu_{sh}/\nu_x > 0.5$. The values of $|\nu_{sh}/\nu_x - 0.5|$ (see Table 2) never exceed 0.02. The largest deviations are present for stars in which broad power excess at subharmonic is observed, like in those plotted in Fig. 10 (OGLE-SMC-CEP-1856, -4255). Still, there is no doubt that the power excess is centred at $1/2\nu_x$ (only the highest peak within the power excess is located a bit off).

Stars that do show power excess at $1/2\nu_x$ are not uniformly distributed in the Petersen diagram. In Fig. 1, stars which show firm power excess at $1/2\nu_x$ are plotted with filled symbols, while for stars in which the detection of power excess is weak are marked with half-filled symbols. Majority of the 48 stars with power excess at $1/2\nu_x$ fall within the middle sequence (40 stars, including 8 weak cases), a few stars fall within the top sequence (8 stars including 6 weak cases) and none falls within the bottom sequence. Thus, 74 per cent of stars from the middle sequence and 31 per cent of the stars from the top sequence show the power excess at $1/2\nu_x$. If we exclude the weak detections, the numbers are 59 and 8 per cent, respectively. We conclude that the occurrence of power excess at $1/2\nu_x$ is strongly correlated with the location of star on the Petersen diagram. The power excess is detected in the majority of stars from the middle sequence, in significantly smaller fraction of stars from the top sequence and in no star from the bottom sequence.

The amplitude of the signal at ν_{sh} is always in the mmag range and is comparable to the amplitude of the signal at ν_x. This is investigated in more detail in Fig. 12, in which in the top panel, we plot the histogram of amplitude ratio, A_{sh}/A_x, and in the bottom panel, we plot A_{sh} versus A_x. The distribution of amplitude ratios is wide, without a pronounced peak. It is truncated at $A_{sh}/A_x \approx 0.5$, which is not surprising. As the signals at ν_x are weak, detected with typical $\mathrm{S/N} \approx 4$–6, we cannot detect the signals with amplitudes significantly lower, below $\approx 0.5A_x$ – these are hidden in the noise. We note eight cases in which peak at ν_{sh} is higher than the peak detected at ν_x. We may safely conclude that amplitudes, A_x and A_{sh}, are comparable. This is further illustrated in the bottom panel of Fig. 12, in which A_{sh} is plotted versus A_x. Green diamonds correspond to stars located within the middle sequence in the Petersen diagram, while blue squares correspond to stars located within the top sequence. The amplitudes are (weakly) correlated; the higher the A_x, the higher the A_{sh}. Amplitudes in stars from the top sequence are in general smaller (see also Section 3.5).

3.5 Possible impact of observational selection effects on incidence rates

The period distribution of stars with additional variability, and the incidence rate of power excess at subharmonic frequency within each sequence, may be affected by observational selection effects. The most important selection effect is related to star's luminosity. On the short-period end, the Cepheids are least luminous (Fig. 7). Therefore, we expect larger noise level in the FT. As a consequence, low-amplitude variability may be hidden in the noise, which could explain the lack of additional variability at ν_x in the shortest period

Table 2. Stars with significant power excess centred at subharmonic frequency, $1/2\nu_x$. Consecutive columns contain: star's id, period ratio, P_x/P_{1O}, frequency of the additional variability, ν_x, frequency of the highest peak detected around $1/2\nu_x$, ν_{sh}, frequency ratio, ν_{sh}/ν_x, amplitude of the additional variability, A_x, and amplitude ratio, A_{sh}/A_x, approximate S/N for the peak at ν_{sh} and remarks: 'weak' – weak detection, 'broad' – broad power excess; 'tdp' – time-dependent pre-whitening of all signals except ν_{sh} conducted.

Star	P_x/P_{1O}	ν_x (1/d)	ν_{sh} (1/d)	ν_{sh}/ν_x	A_x (mag)	A_{sh}/A_x	S/N	Remarks
OGLE-SMC-CEP-0212	0.6247	0.919 40(4)	0.460 17(4)	0.5005	0.0035	0.95	4.0	
OGLE-SMC-CEP-0251	0.6249	0.890 65(1)	0.447 22(1)	0.5021	0.0039	1.02	6.5	
OGLE-SMC-CEP-0628	0.6231	0.871 58(2)	0.429 11(2)	0.4923	0.0032	1.13	6.1	
OGLE-SMC-CEP-0708	0.6291	1.234 06(2)	0.609 76(3)	0.4941	0.0034	0.68	3.8	tdp, weak
OGLE-SMC-CEP-0866	0.6223	0.921 66(2)	0.458 84(2)	0.4978	0.0027	0.81	4.1	tdp, weak
OGLE-SMC-CEP-1119	0.6260	0.962 30(2)	0.484 10(2)	0.5031	0.0042	1.11	6.2	
OGLE-SMC-CEP-1127	0.6270	0.973 48(3)	0.483 76(3)	0.4969	0.0033	0.90	4.2	
OGLE-SMC-CEP-1366	0.6224	0.754 93(3)	0.389 02(4)	0.5153	0.0034	0.68	4.1	tdp, broad
OGLE-SMC-CEP-1516	0.6248	0.819 94(4)	0.416 72(4)	0.5082	0.0021	0.93	3.7	weak
OGLE-SMC-CEP-1710	0.6217	0.760 26(1)	0.374 68(2)	0.4928	0.0031	0.56	4.7	tdp
OGLE-SMC-CEP-1771	0.6391	0.575 12(2)	0.286 87(3)	0.4988	0.0022	0.59	4.1	tdp, weak
OGLE-SMC-CEP-1773	0.6249	0.781 02(2)	0.388 92(2)	0.4980	0.0026	0.82	4.2	tdp, broad
OGLE-SMC-CEP-1856	0.6223	0.846 51(1)	0.433 73(2)	0.5124	0.0046	0.45	4.1	tdp, broad
OGLE-SMC-CEP-1870	0.6333	0.400 92(1)	0.197 50(2)	0.4926	0.0026	0.52	4.5	tdp
OGLE-SMC-CEP-1975	0.6235	0.840 83(3)	0.423 08(3)	0.5032	0.0028	0.89	4.4	
OGLE-SMC-CEP-2178	0.6199	0.651 49(2)	0.325 76(3)	0.5000	0.0029	0.84	4.9	
OGLE-SMC-CEP-2227	0.6207	0.776 45(2)	0.390 90(2)	0.5034	0.0024	0.73	4.3	
OGLE-SMC-CEP-2253	0.6356	0.454 60(2)	0.229 36(2)	0.5045	0.0023	0.77	3.9	weak
OGLE-SMC-CEP-2285	0.6240	0.793 24(2)	0.407 05(2)	0.5131	0.0033	0.69	4.3	tdp, broad
OGLE-SMC-CEP-2433	0.6409	0.652 98(2)	0.326 04(2)	0.4993	0.0032	0.74	4.0	weak
OGLE-SMC-CEP-2567	0.6207	0.712 86(3)	0.354 88(3)	0.4978	0.0041	0.76	4.4	
OGLE-SMC-CEP-2594	0.6222	0.772 03(2)	0.386 37(3)	0.5005	0.0043	0.90	5.7	
OGLE-SMC-CEP-2627	0.6212	0.775 97(2)	0.392 51(2)	0.5058	0.0038	0.62	4.1	tdp, broad, weak
OGLE-SMC-CEP-2628	0.6228	0.919 35(2)	0.459 04(3)	0.4993	0.0028	0.78	3.9	weak
OGLE-SMC-CEP-2681	0.6228	0.773 27(1)	0.376 18(2)	0.4865	0.0047	0.57	4.1	broad
OGLE-SMC-CEP-2805	0.6179	0.705 17(2)	0.340 70(3)	0.4831	0.0036	0.83	5.1	
OGLE-SMC-CEP-2813	0.6204	0.710 32(1)	0.357 81(2)	0.5037	0.0030	0.98	5.4	
OGLE-SMC-CEP-3040	0.6393	0.627 20(2)	0.316 10(2)	0.5040	0.0025	0.67	4.0	weak
OGLE-SMC-CEP-3172	0.6242	0.963 61(2)	0.474 73(2)	0.4927	0.0031	0.74	4.2	broad
OGLE-SMC-CEP-3239	0.6219	0.894 78(3)	0.456 43(4)	0.5101	0.0046	0.55	3.6	weak
OGLE-SMC-CEP-3292	0.6189	0.645 90(2)	0.329 66(3)	0.5104	0.0026	0.57	3.9	tdp, weak, broad
OGLE-SMC-CEP-3298	0.6389	0.583 97(2)	0.290 91(2)	0.4982	0.0023	0.88	5.3	
OGLE-SMC-CEP-3312	0.6234	0.757 52(2)	0.368 21(2)	0.4861	0.0029	0.79	4.3	broad
OGLE-SMC-CEP-3317	0.6244	0.800 69(3)	0.397 38(1)	0.4963	0.0029	1.08	5.1	
OGLE-SMC-CEP-3343	0.6250	0.873 48(1)	0.438 12(2)	0.5016	0.0047	0.76	6.3	
OGLE-SMC-CEP-3349	0.6261	0.830 96(2)	0.422 82(3)	0.5088	0.0031	0.81	4.3	broad
OGLE-SMC-CEP-3590	0.6241	0.798 12(1)	0.405 93(2)	0.5086	0.0027	0.62	3.9	tdp, weak, broad
OGLE-SMC-CEP-3944	0.6232	0.742 17(2)	0.366 15(2)	0.4933	0.0028	1.09	6.0	broad
OGLE-SMC-CEP-3987	0.6350	0.467 44(2)	0.238 51(3)	0.5102	0.0039	0.57	4.3	tdp, weak
OGLE-SMC-CEP-4011	0.6256	0.880 95(2)	0.435 34(3)	0.4942	0.0035	0.98	5.4	
OGLE-SMC-CEP-4046	0.6217	0.715 27(2)	0.359 77(3)	0.5030	0.0044	0.75	5.2	
OGLE-SMC-CEP-4068	0.6205	0.801 52(2)	0.402 38(2)	0.5020	0.0034	1.03	6.2	broad
OGLE-SMC-CEP-4205	0.6236	0.824 50(2)	0.412 26(3)	0.5000	0.0059	0.64	5.5	
OGLE-SMC-CEP-4255	0.6246	0.765 57(3)	0.371 50(4)	0.4853	0.0039	0.76	4.3	broad
OGLE-SMC-CEP-4262	0.6226	0.767 36(3)	0.384 11(4)	0.5006	0.0041	0.85	4.2	
OGLE-SMC-CEP-4388	0.6226	0.789 52(3)	0.395 29(3)	0.5007	0.0045	1.11	5.7	
OGLE-SMC-CEP-4395	0.6373	0.546 82(3)	0.274 16(4)	0.5014	0.0033	0.75	4.1	weak
OGLE-SMC-CEP-4462	0.6201	0.754 81(3)	0.376 36(3)	0.4986	0.0030	1.09	5.2	

first overtone stars or lack of subharmonics in stars of the bottom sequence in the Petersen diagram. On long-period end, the stars are more luminous and the noise level should be lower.

To quantify the impact of noise on the detection of low-amplitude variability, we first estimate the noise level in the FT as a function of pulsation period. To this aim, we analysed the data for all SMC OGLE-III 1O Cepheids in the following, homogeneous way. Using the time-dependent pre-whitening on a season-to-season basis we removed from the data (possibly non-stationary) variability associated with the first overtone (sixth-order Fourier series). This technique also removes trends possibly present in the data. Possible signals at ν_x and at $1/2\nu_x$ remain in the data but, as these signals are of low amplitude and present in less than 10 per cent of all 1O Cepheids, they should not alter our estimate significantly. Then, in the frequency spectrum of residual data for each star, we computed the average noise level in the frequency range $(0, 3\nu_{1O})$. The resulting data, noise versus first overtone period, were fitted with spline function. This function, multiplied by 4, is plotted with dashed line in Fig. 13 and represents the estimate of the detection threshold as a function of the first overtone period.

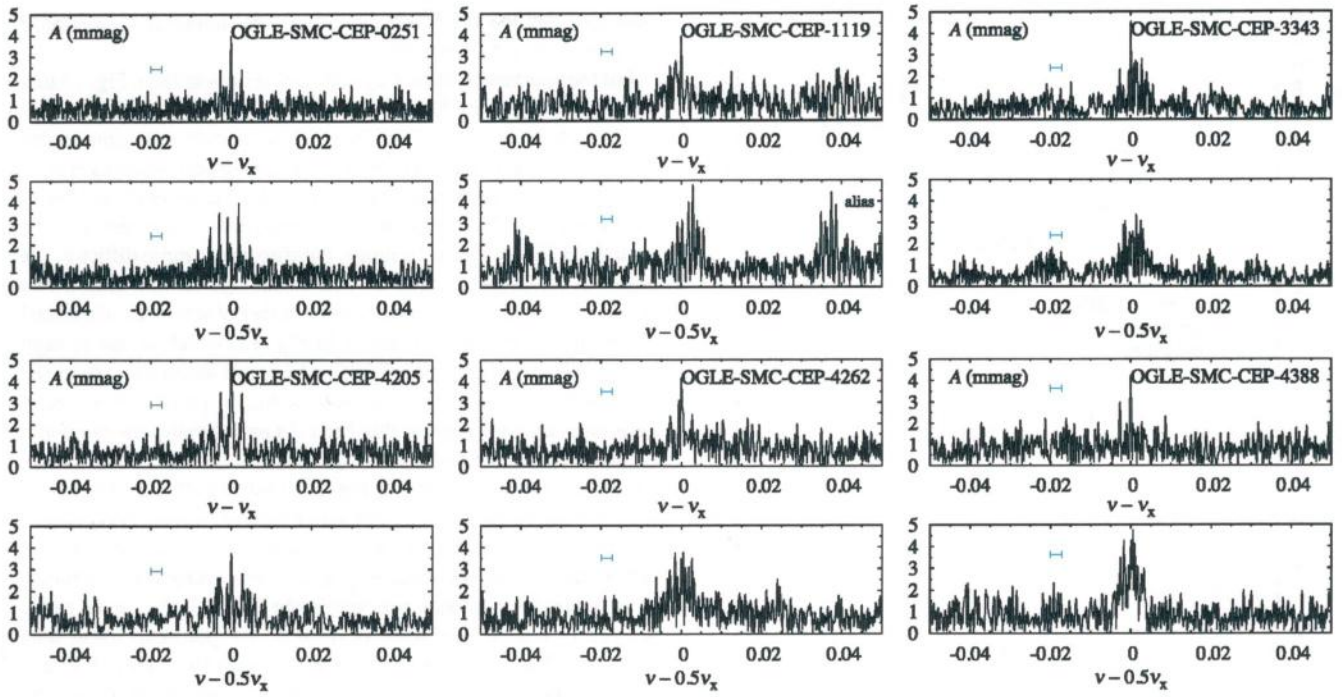

Figure 9. Frequency spectra for selected stars with additional variability present at ν_x and simultaneously with significant power excess centred at $1/2\nu_x$. In the top panel, a section of frequency spectrum centred at ν_x is plotted. In the bottom panel, a section of frequency spectrum centred at $\nu_x/2$ is plotted. The frequency range is the same in two panels. The extent of the horizontal bar plotted in each panel (at S/N = 4.0) corresponds to separation expected for 1-yr aliases.

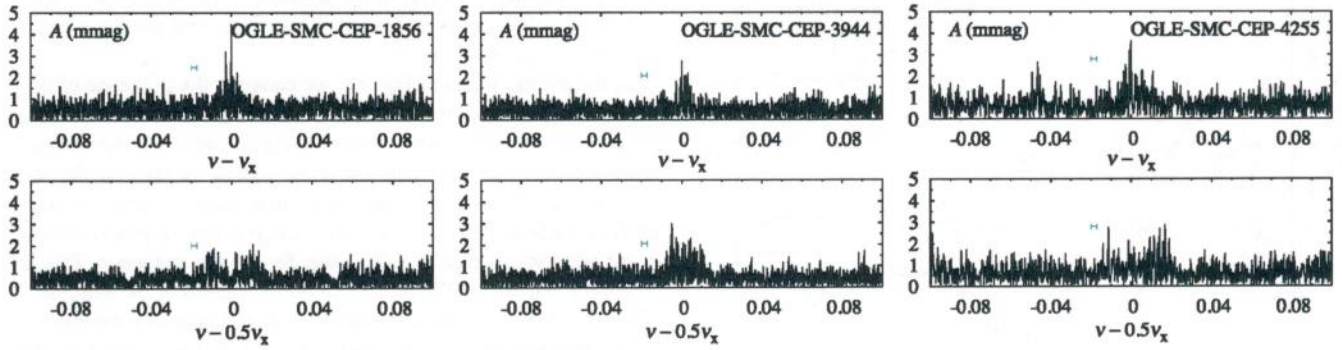

Figure 10. The same as Fig. 9, but for stars with broad power excess at subharmonic frequency.

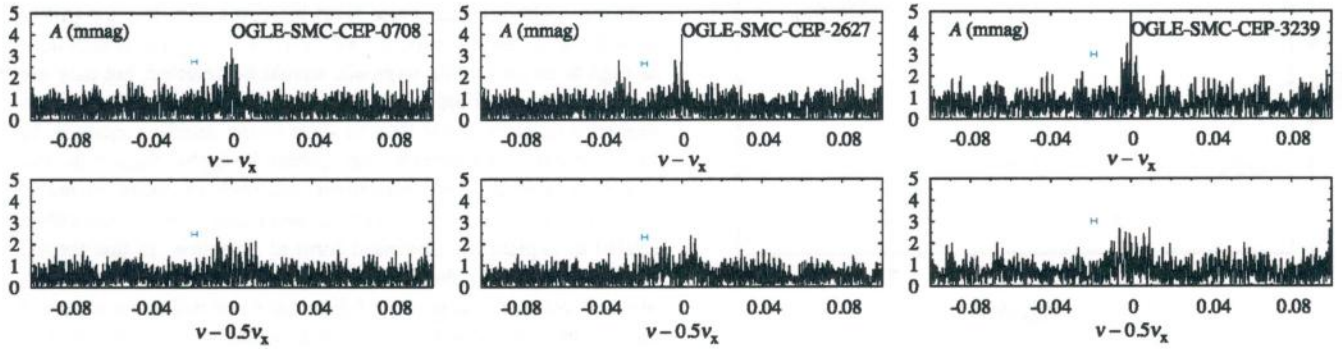

Figure 11. The same as Fig. 9, but for stars with weak detection of power excess at subharmonic frequency.

In the top panel of Fig. 13, we consider the influence of selection effects on the detection of additional variability at ν_x. Different symbols represent the data for the three sequences. As noted in Section 3.2 (see also Fig. 4), the discussed form of pulsation is not present for $P_{1O} < 0.75$ d and is very scarce in the $0.75\,\mathrm{d} < P_{1O} < 1$ d range in which 1O Cepheids are very numerous. The question we can answer is, whether the sharp decrease of the incidence rate at shorter periods can be explained by observational selection,

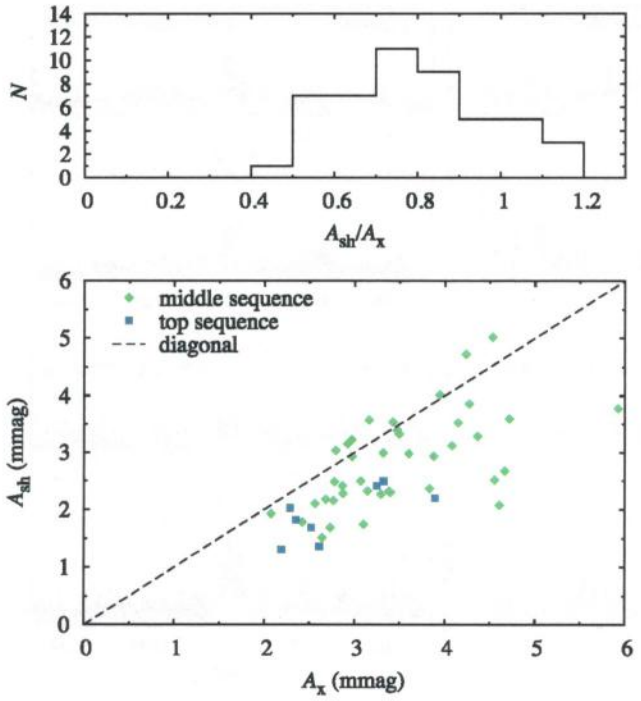

Figure 12. Histogram of amplitude ratios A_{sh}/A_x (top panel) and plot of A_{sh} versus A_x (bottom panel).

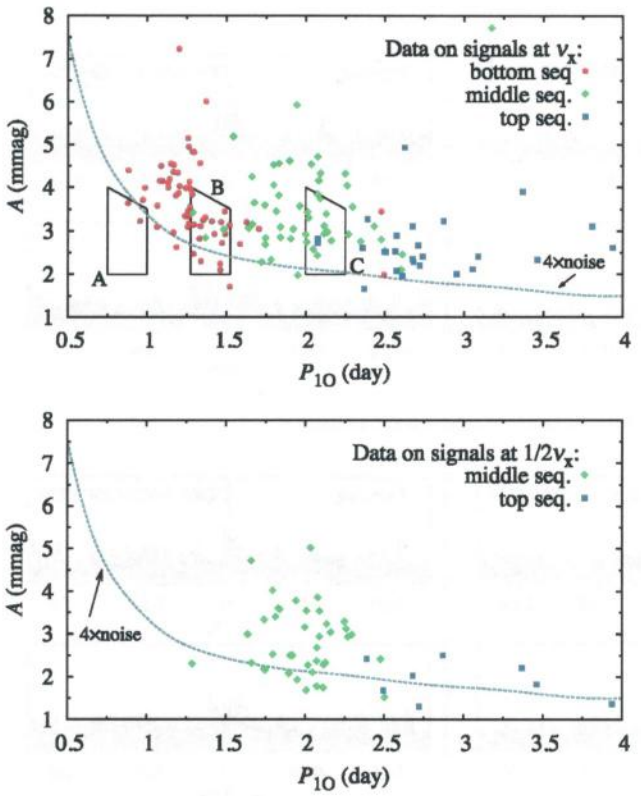

Figure 13. The influence of the observational selection effects on the period distribution of stars with the additional variability at ν_x (top panel) and on the incidence rate of power excess at $1/2\nu_x$ for stars of the three sequences in the Petersen diagram (bottom panel).

assuming that the amplitude distribution of signals at ν_x is similar as is observed for longer periods.

For the shortest periods, $P_{1O} < 0.75$ d, it is clear from Fig. 13 that the noise level is very high. It strongly depends on pulsation period, but already at $P_{1O} = 0.75$ d detection of signals with amplitudes below 4.5 mmag might be difficult and situation worsens fast as period is decreased further. Thus, the lack of additional variability for the $P_{1O} < 0.75$ d range may be entirely due to selection effects.

In the $0.75\,\mathrm{d} < P_{1O} < 1\,\mathrm{d}$ range, the situation is more difficult. We note that for longer periods we can detect signals with amplitudes above ~2 mmag. Thus, the very low number of stars with additional variability located within box A in Fig. 13, which is due to high noise level, may be responsible for the small incidence rate in the discussed period range as compared to longer periods. How many detections may we miss in this box? As an estimate, we can count the stars within the same area, but at longer periods, for example, within boxes marked B or C in Fig. 13. There are 21 stars within box B and 15 stars within box C. These numbers are scaled by N_A/N_B or N_A/N_C factor, where N_X is the total number of 1O Cepheids within period range corresponding to a given box. Using these numbers to estimate the incidence rate within the $0.75\,\mathrm{d} < P_{1O} < 1\,\mathrm{d}$ range we get 11.1 ± 1.7 per cent or 14.6 ± 1.9 per cent, using data from box B or C, respectively. We conclude that sharp decrease of the incidence rate at $P_{1O} < 1$ d may be entirely explained by observational selection.

For the period range characteristic for the middle and top sequences in the Petersen diagram, the noise level is roughly the same, it slowly decreases with increasing period. Thus, a small decrease of the incidence rate of the discussed form of pulsation, with pulsation period, noted in Section 3.2, is likely real and not a result of observational selection.

In the bottom panel of Fig. 13, we consider the influence of observational selection on the incidence rate of power excess at $1/2\nu_x$ within the three sequences. Symbols correspond to observational data. We first note that amplitudes of signals in stars of the top sequence are, on average, lower than amplitudes of signals in stars of the middle sequence. Also, the incidence rate of power excess at subharmonic is significantly lower for the top sequence. This is obviously not due to different noise levels; signals of the amplitude characteristic for the middle sequence should be easily detected at longer periods. The possible explanation is that amplitudes of the signals at $1/2\nu_x$ in stars of the top sequence are lower than in stars of the middle sequence. Situation is similar for the stars of the bottom sequence. Although the noise level increases with the decreasing period, the increase is pronounced only for $P_{1O} \lesssim 1$ d. Amplitudes as high as in the middle sequence should be detected, but they are not. Thus, the amplitudes of signals at $1/2\nu_x$ in stars of the bottom sequence must be lower than in stars of the middle sequence. In fact, to remain undetectable, they cannot be higher than in the top sequence. The sequence-dependent amplitude of power excess at $1/2\nu_x$ is in line with the theory proposed recently by Dziembowski (2016) to explain the discussed form of pulsation. In this theory, the signals at $1/2\nu_x$ should be observed for all sequences and correspond to non-radial modes of different ℓ, for which the observed amplitudes differ due to geometric cancellation. We discuss it in more detail in Section 4.2.

3.6 Time-variability

Complex, non-coherent, and often broad structures, detected both at ν_x and in some stars at $1/2\nu_x$ (Figs 9, 10 and 11), indicate strong time variation of the amplitude and/or phase of the variability these

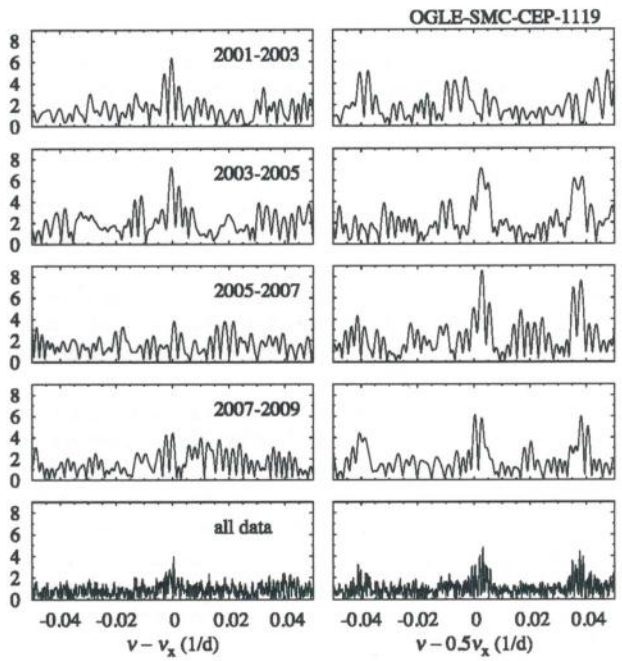

Figure 14. Seasonal analysis of the frequency spectra centred at ν_x (left-hand panels) and at $1/2\nu_x$ (right-hand panels) for OGLE-SMC-CEP-1119. The bottom panels show the frequency spectra for all data. Structure at $\nu - 0.5\nu_x \approx 0.04$ (in the right-hand panels) is a daily alias of structure centred at $0.5\nu_x$.

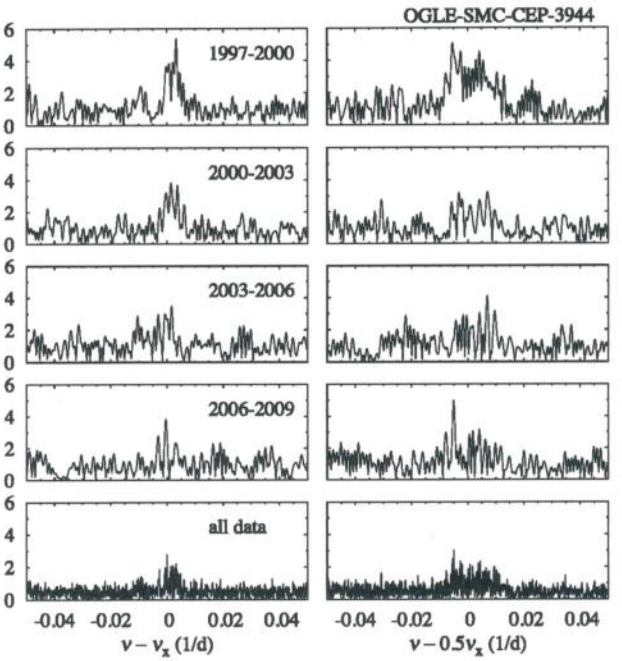

Figure 15. Same as Fig. 14, but for OGLE-SMC-CEP-3944.

structures represent. Because of the low amplitudes of these signals, typically between 2 and 5 mmags, and relatively high noise level in the ground-based observations, it is difficult to analyse this variability in more detail, with high time resolution. Still, some analysis is possible for stars in which the signals are detected at relatively high S/N. For these stars, we divided the data into four groups, each consisting of two (or in some cases three) observing seasons. Then for each group, we calculated the discrete FT and investigated the frequency spectrum at around ν_x and $1/2\nu_x$. Results of the analysis are presented in Fig. 14 (for OGLE-SMC-CEP-1119) and in Fig. 15 (for OGLE-SMC-CEP-3944). Results are qualitatively similar for a few other stars for which such analysis was possible.

In Fig. 14, we observe that from season to season the amplitude and location of the peaks present at ν_x and at $1/2\nu_x$ strongly vary. In particular, the signal at ν_x is significant in 2001–2005 seasons, while it is not significant later on. The signal at $1/2\nu_x$ was insignificant in the first observing seasons, while it was clearly present starting from 2003 and later on.

For OGLE-SMC-CEP-3944, analysed in Fig. 15, we observe that signal at ν_x is always present, but its amplitude and/or phase clearly vary. The signal at $1/2\nu_x$ is weakly marked in between 2000 and 2006. Structure of the observed broad power excess vary in time. As a result, broad and essentially flat power excess is present in the analysis of all data.

4 DISCUSSION

4.1 Comparison with RR Lyr stars

A very similar form of variability is detected in RRc stars, as already mentioned in the Introduction. The obvious similarity is the characteristic period ratio, which falls into similar range, $P/P_{1O} \in (0.60, 0.65)$, and the occurrence of the additional variability in first overtone stars (or in double-mode stars, with fundamental and first overtone modes simultaneously excited). The present study allow a more detailed comparison.

(i) Incidence rate of the phenomenon: the phenomenon is common among RRc stars; space observations leave no doubt; 14 out of 15 RRc/RRd stars observed from space show the phenomenon (see Moskalik et al. 2015). Incidence rates in the top-quality ground-based observations are also high, 27 per cent in the Galactic bulge sample of RRc stars studied by Netzel et al. (2015b) and 38 per cent in the M3 sample observed by Jurcsik et al. (2015). Unfortunately, for Cepheids, we lack systematic analysis of large sample of stars. The 138 stars considered here constitute 8.4 per cent of the OGLE-III sample of 1O SMC Cepheids. The incidence rate depends on the pulsation period; in particular the phenomenon does not occur in the shortest period ($P_{1O} \lesssim 0.8$ d) Cepheids. For longer periods, the incidence rate is ≈8–15 per cent. Space observations of 1O Cepheids are scarce. Polaris was observed with star tracker on board *Coriolis* satellite (Bruntt et al. 2008), SZ Tau was observed with *MOST* (Evans et al. 2015) and two other stars were observed with *CoRoT* (Poretti et al. 2015). In these stars, additional variability was not detected. Two stars observed with *K2* show the discussed form of pulsation (Plachy et al., in preparation).

(ii) The Petersen diagram: both for Cepheids and for RR Lyr stars, three sequences are present – see Fig. 16. The Cepheid sequences are slanted and well separated. The bottom sequence is most populated, but the middle and top sequences are well represented, too. In the case of RR Lyr stars, the sequences are nearly horizontal, not that well separated and majority of stars fall within the bottom sequence. In both groups, stars that belong to more than one sequence are found. While in the case of RR Lyr stars, there are very good examples of stars that belong to three sequences simultaneously (see fig. 5 in Netzel et al. 2015b), in the case of Cepheids only stars that belong to two sequences are found, and these are rather weak cases (Fig. 3).

(iii) Amplitudes: both in Cepheids and in RR Lyr stars, the additional periodicity is of low amplitude, in the mmag range. In both

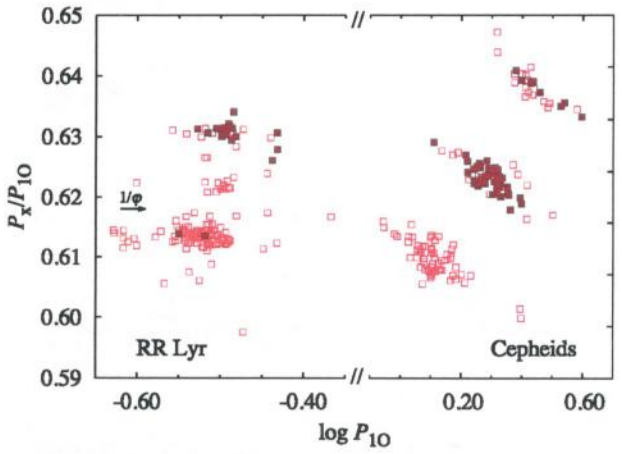

Figure 16. Petersen diagram with RRc stars with additional periodicity from Netzel et al. (2015b) and 1O Cepheids from the present study. Filled symbols correspond to stars with power excess detected at $1/2\nu_x$. Arrow indicates the reciprocal of the golden ratio.

cases, the most typical amplitude is around 2 per cent of the first overtone amplitude [compare fig. 7 in Netzel et al. (2015b) and Fig. 6].

(iv) Subharmonics: both in Cepheids and in RR Lyr stars, significant power excess centred at $1/2\nu_x$ is detected. Subharmonics are detected in 20 per cent of the sample of Galactic bulge RRc stars with additional variability analysed by Netzel et al. (2015b) and in 35 per cent of the present Cepheid sample. Netzel et al. (2015b) reported the power excess also at $3/2\nu_x$, other cases are known from space observations (see e.g. Molnár et al. 2015; Moskalik et al. 2015; Kurtz et al. 2016). No firm detection of power excess at $3/2\nu_x$ is found in the present Cepheid sample. Stars with power excess at $1/2\nu_x$, both RR Lyr and Cepheids, are not uniformly distributed in the Petersen diagram. This is illustrated in Fig. 16 in which we plot the stars from the present sample of SMC Cepheids and from the study of Netzel et al. (2015b) (see also Netzel, Smolec & Moskalik 2016); stars with power excess at subharmonic are marked with filled symbols.

(v) Time variability of the additional signals: both for Cepheids and for RR Lyr stars, the signals at ν_x and at $1/2\nu_x$ are complex: power excesses, or clusters of peaks (sometimes very broad) are detected, rather than single and coherent peaks. Compare fig. 11 in Netzel et al. (2015b) and fig. 2 in Netzel et al. (2016) with Figs 9, 10 and 11. Such complex structures present in the frequency spectrum correspond to strong and irregular variability of signal's phase and/or amplitude.

4.2 Nature of the additional variability

Based on the just presented comparison we conclude, that the double-periodic pulsation observed both in RRc stars and in 1O Cepheids, with characteristic period ratios, $P_x/P_{1O} \in (0.60, 0.65)$, is qualitatively very similar. Consequently, nature of the additional variability and mechanism of its excitation are most likely the same. In both cases, it cannot be pulsation in two radial modes (Dziembowski & Smolec 2009; Moskalik et al. 2015). A model or theory common for the two groups should be searched for.

Dziembowski (2012) proposed an explanation for Cepheids. The additional variability at ν_x was interpreted as a non-radial f mode of high angular degree. The three Cepheid sequences were reproduced assuming that additional modes have $\ell = 42$ (top sequence), 46 (middle sequence) and 50 (bottom sequence). Due to geometric cancellation, modes of such large angular degree are expected to have very low observed amplitudes. Two problems arise then, however. First, the geometric cancellation is lower for even-ℓ modes and, at high degrees, is roughly the same for these modes (depends only on mode parity). Hence, if $\ell = 42$, 46 and 50 are observed, then $\ell = 44$ and 48 should be observed as well (all these modes are linearly unstable), which is not the case. Secondly, the required intrinsic amplitudes are very high, implying large broadening of the spectral lines. Both problems are discussed in Dziembowski (2012). When this model was proposed, it was not known that in these stars subharmonics are detected. RR Lyr stars were not studied by Dziembowski (2012).

Lindner et al. (2015) focused on RR Lyr stars, in particular on one star observed by *Kepler* (KIC5520878) and noticed that its period ratio is close to the reciprocal of the golden ratio, $1/\varphi \approx 0.618$. Lindner et al. (2015) argue that the dynamics driven by two frequencies in the golden ratio maximally resist perturbations. As noted by Smolec, Netzel & Soszyński (2016) and also well visible in Fig. 16, in which we mark $1/\varphi$ with an arrow, the stars avoid the golden ratio. In our opinion, the proximity of period ratio to $1/\varphi$ in some RR Lyr stars is a pure coincidence.

Recently, Dziembowski (2016) proposed a new explanation, in which the signal observed at $1/2\nu_x$ corresponds to non-radial, $\ell = 7 - 9$ modes. The signal at ν_x is its harmonic, which gains the significant amplitude due to non-linear, quadratic effect. According to this model, stars in which subharmonics are detected should not be distributed uniformly among sequences visible in the Petersen diagram. As geometric cancellation is lower for even-ℓ modes, we should observe the power excess at subharmonic, i.e. we should detect the true non-radial mode, preferentially in sequences which correspond to even-ℓ pulsation. In the case of Cepheids, it is the middle sequence ($\ell = 8$; $\nu_x = 2\nu_8$). The top sequence corresponds to $\ell = 7$, while the lower sequence to $\ell = 9$. Geometric cancellation is slightly lower for $\ell = 7$ than for $\ell = 9$. In Fig. 16, we observe a nice qualitative confirmation of this theory for Cepheids.

In the case of RR Lyr stars, the top sequence corresponds to even ℓ ($\ell = 8$) and subharmonic detection (non-radial $\ell = 8$ mode detection) should be more common there. According to the Dziembowski (2016) theory, the bottom, most populated sequence for RR Lyr stars, corresponds to odd-ℓ mode ($\ell = 9$). The weakly marked middle sequence corresponds to the combination frequency ($\nu_8 + \nu_9$) and no subharmonics should be detected there. This is indeed what we observe – Fig. 16. Detailed description of the model is in preparation (Dziembowski & Smolec, in preparation)

5 SUMMARY

We have analysed 138 1O Cepheids from the SMC in which Soszyński et al. (2010) reported additional variability with $P/P_{1O} \in (0.60, 0.65)$. These stars form three sequences in the Petersen diagram. Our most important findings are the following.

(i) The three sequences in the Petersen diagram are not equally populated. In 64 stars, we detect periodicities corresponding to the bottom sequence, in 54 stars, corresponding to the middle sequence, and in 26 stars, corresponding to the top sequence. The numbers do not add up to 138, as in the frequency spectra of six stars, we detect two significant periodicities that correspond to two of the three sequences.

(ii) The additional variability is always of low amplitude, typically about 2–4 per cent of the first overtone amplitude (between 2 and 5 mmag) – Figs 5 and 6.

(iii) In 35 per cent of stars (25 per cent if weak cases are excluded), we detect power excess centred at $1/2\nu_x$, i.e. at subharmonic. The power excess is often broad and of complex structure (Figs 9 and 10). Amplitude of the signal detected at $1/2\nu_x$ is comparable to amplitude of the signal detected at ν_x – Fig. 12.

(iv) Stars in which power excess at subharmonic is detected are not uniformly distributed in the Petersen diagram – Figs 1 and 16. Subharmonics are detected most frequently in the stars of the middle sequence (in 74 per cent of stars; 59 per cent excluding weak cases). Incidence rate is much lower for the top sequence (31 per cent or 8 per cent without weak cases). Subharmonics are not detected in stars of the bottom sequence.

(v) The additional variability (both at ν_x and at $1/2\nu_x$) is strongly non-stationary; its amplitude and/or phase, strongly vary in time (Figs 14 and 15).

(vi) A similar form of pulsation, in which radial first overtone and additional low-amplitude variability is detected with period ratios $P_x/P_{1O} \in (0.60, 0.65)$, is also present in RR Lyr stars. A detailed comparison we have done indicates, that the nature of this phenomenon is most likely the same in both groups of classical pulsators. Therefore, a common theory to explain this puzzling form of pulsation should be searched for.

(vii) In the Petersen diagram, the distribution of stars in which power excess at subharmonic is detected is not uniform, both for Cepheids and for RR Lyr stars (Fig. 16). The observed distribution favors the model proposed recently by Dziembowski (2016) (Section 4.2).

It is very important to establish the incidence rate of the discussed form of pulsation in Cepheids, to check whether it is as common as in RR Lyr stars. The systematic search in the OGLE data was started. It seems crucial however, to observe 1O Cepheids from space with *K2* mission. High-precision photometry it gathers, offers the possibility to detect periodicities of very low amplitude. Detection of power excess at subharmonic frequencies for stars that belong to different sequences, and study of the amplitude distribution of these signals, is crucial to test the model proposed by Dziembowski (2016).

ACKNOWLEDGEMENTS

This research is supported by the Polish National Science Centre through grants DEC-2012/05/B/ST9/03932 and DEC-2015/17/B/ST9/03421. We are grateful to Paweł Moskalik for detailed reading of the manuscript and many comments that significantly improved its content. Fruitful and stimulating discussions with Wojtek Dziembowski are acknowledged. We acknowledge the summer student program at Nicolaus Copernicus Astronomical Center during which part of this work was completed.

REFERENCES

Alcock C. et al., 2003, ApJ, 598, 597
Berdnikov L. N., Pastukhova E. N., 1994, Astron. Lett., 20, 479
Berdnikov L. N., Ignatova V. V., Pastukhova E. N., Turner D. G., 1997, Astron. Lett., 23, 177
Bruntt H. et al., 2008, ApJ, 683, 433
Dziembowski W., 2012, Acta Astron., 62, 323
Dziembowski W., 2016, preprint (arXiv:1512.03708)
Dziembowski W., Smolec R., 2009, in Guzik J. A., Bradley P. A., eds, AIP Conf. Proc. Vol. 1170, Stellar Pulsation: Challenges For Theory And Observation. Am. Inst. Phys., New York, p. 83
Evans N. R. et al., 2015, MNRAS, 446, 4008
Jurcsik J. et al., 2015, ApJS, 219, 25
Kurtz D. W., Bowman D. M., Ebo S. J., Moskalik P., Handberg R., Lund M. N., 2016, MNRAS, 455, 1237
Lindner J. F., Kohar V., Kia B., Hippke M., Learned J. G., Ditto W. L., 2015, Phys. Rev. Lett., 114, 054101
Molnár L. et al., 2015, MNRAS, 452, 4283
Moskalik P., 2014, in Guzik J. A., Chaplin W. J., Handler G., Pigulski A., eds, IAU Symp. 301, Precision Asteroseismology. Kluwer, Dordrecht, p. 249
Moskalik P., Kołaczkowski Z., 2009, MNRAS, 394, 1649
Moskalik P., Kołaczkowski Z., Mizerski T., 2004, in Kurtz D. W., Pollard K., eds, ASP Conf. Ser. Vol. 310, IAU Colloq. 193: Variable Stars in the Local Group. Astron. Soc. Pac, San Francisco, p. 498
Moskalik P. et al., 2015, MNRAS, 447, 2348
Netzel H., Smolec R., Moskalik P., 2015a, MNRAS, 447, 1173
Netzel H., Smolec R., Moskalik P., 2015b, MNRAS, 453, 2022
Netzel H., Smolec R., Moskalik P., 2016, preprint (arXiv:1601.08096)
Pietrukowicz et al., 2013, Acta Astron., 63, 379
Poleski R., 2008, Acta Astron., 58, 313
Poretti E., Le Borgne J. F., Rainer M., Baglin A., Benkő J. M., Debosscher J., Weiss W. W., 2015, MNRAS, 454, 849
Poretti E., Baglin A., Weiss W.W., ApJ, 795, L36
Simon N. R., Lee A. S., 1981, ApJ, 248, 291
Smolec R., Netzel H., Soszyński I., 2016, Highlights of Astronomy, Vol. 17. in press
Soszyński I. et al., 2008a, Acta Astron., 58, 153
Soszyński I. et al., 2008b, Acta Astron., 58, 163
Soszyński I. et al., 2010, Acta Astron., 60, 17
Soszyński I. et al., 2011, Acta Astron., 61, 285
Soszyński I. et al., 2015, Acta Astron., 65, 329
Szabó R., Benkő J. M., Paparó M., 2014, A&A, 570, A100
Udalski A., Szymański M. K., Soszyński I., Poleski R., 2008, Acta Astron., 58, 69
Udalski A., Szymański M. K., Szymański G., 2015, Acta Astron., 65, 1

APPENDIX A: STARS WITH ADDITIONAL VARIABILITY

Table A1 list all the stars analysed in the present study and contains their basic properties.

APPENDIX B: COMPARISON WITH SOSZYŃSKI ET AL. (2010)

For each star Soszyński et al. (2010) (S10 in the following) provided two periods, P_{1O} and P_x, and these are the only quantities we can compare. For the majority of stars, there is an excellent agreement between our studies. In six stars, the small differences are a consequence of the complex form in which additional variability appears in the frequency spectrum (see Fig. 2 and Section 3.1) – two close peaks of similar height or cluster of peaks. Small differences in the analysis (detrending, outlier rejection) may slightly alter the relative height of the peaks and lead to slightly different frequencies adopted in the two studies. The difference in the resulting period ratios is negligible however. Two examples are illustrated in the top two panels of Fig. 2 in which filled diamonds mark the frequency adopted in this study and open diamonds mark the frequency adopted in S10.

More significant differences are due to alias ambiguities and are found for six stars, described below on a star-by-star basis. Still, only for one star the period ratios in the two studies differ by 3 per cent. For five other stars, the difference is less than 1 per cent.

Table A1. Properties of first overtone Cepheids with additional variability. The consecutive columns contain: star's id, first overtone period, P_{1O}, period of the additional variability, P_x, period ratio, P_x/P_{1O}, amplitude of the first overtone, A_{1O}, and amplitude ratio, A_x/A_{1O}, and remarks: 'al' – daily alias of signal at ν_x is higher; 'nsx' – complex appearance of the signal at ν_x; 'nsO' – non-stationary first overtone; 'cf' – combination frequency of ν_x and ν_{1O} detected; 'sh' – power excess at sub-harmonic frequency (around $1/2\nu_x$) detected ('*sh*' – weak detection); 'ap' – additional periodicity detected; 'tdp' – time-dependent analysis was conducted; '?' – weak detection (S/N given in the parenthesis).

Star	P_{1O} (d)	P_x (d)	P_x/P_{1O}	A_{1O} (mag)	A_x/A_{1O}	Remarks
OGLE-SMC-CEP-0056	0.986 0208(7)	0.603 73(1)	0.6123	0.1689	0.024	? (S/N = 3.77)
OGLE-SMC-CEP-0212	1.741 010(4)	1.087 66(4)	0.6247	0.0997	0.036	sh, nsx
OGLE-SMC-CEP-0251	1.796 802(1)	1.122 79(2)	0.6249	0.1399	0.029	sh, nsx
OGLE-SMC-CEP-0280	1.675 191(1)	1.043 44(2)	0.6229	0.1377	0.026	nsO, ap
OGLE-SMC-CEP-0281	1.266 2457(7)	0.774 075(9)	0.6113	0.1263	0.033	al, nsx
OGLE-SMC-CEP-0307	0.973 4743(7)	0.597 18(1)	0.6134	0.1922	0.019	nsO, ap
OGLE-SMC-CEP-0447	1.265 1448(8)	0.776 24(1)	0.6136	0.1300	0.024	nsO, nsx
OGLE-SMC-CEP-0456	0.877 6927(4)	0.540 588(7)	0.6159	0.1579	0.023	nsO, tdp, ? (S/N = 3.93)
OGLE-SMC-CEP-0466	1.131 7607(5)	0.690 278(8)	0.6099	0.1603	0.026	al
OGLE-SMC-CEP-0491	1.064 1278(4)	0.6527 31(8)	0.6134	0.1679	0.021	
OGLE-SMC-CEP-0509	1.626 176(1)	0.984 94(2)	0.6057	0.1322	0.024	ap
OGLE-SMC-CEP-0592	1.149 5482(9)	0.702 313(9)	0.6109	0.1371	0.033	al, nsO, nsx
OGLE-SMC-CEP-0628	1.841 217(1)	1.147 33(2)	0.6231	0.1385	0.022	sh, nsx, nsO
OGLE-SMC-CEP-0631	2.346 706(4)	1.467 74(6)	0.6254	0.1253	0.022	al, ap
OGLE-SMC-CEP-0680	1.483 925(1)	0.930 37(2)	0.6270	0.1296	0.023	nsO
OGLE-SMC-CEP-0696	2.359 034(2)	1.510 60(4)	0.6403	0.1065	0.024	nsO, nsx
OGLE-SMC-CEP-0708	1.288 1769(6)	0.810 34(1)	0.6291	0.1738	0.020	al, *sh*, nsx
OGLE-SMC-CEP-0759	1.261 5578(6)	0.770 574(7)	0.6108	0.1450	0.034	nsO, nsx
OGLE-SMC-CEP-0797	2.623 163(3)	1.671 74(2)	0.6373	0.0840	0.059	al, nsO, nsx, cf, ap
OGLE-SMC-CEP-0800	1.259 8153(8)	0.770 40(2)	0.6115	0.1683	0.020	
OGLE-SMC-CEP-0828	1.179 8295(9)	0.714 330(9)	0.6055	0.1040	0.037	nsO
OGLE-SMC-CEP-0833	1.132 8767(6)	0.692 37(1)	0.6112	0.1467	0.027	nsO
OGLE-SMC-CEP-0841	1.353 5878(8)	0.822 78(1)	0.6079	0.1495	0.022	nsx
OGLE-SMC-CEP-0844	1.256 0636(5)	0.770 35(1)	0.6133	0.1488	0.023	nsx
OGLE-SMC-CEP-0866	1.743 531(1)	1.085 00(3)	0.6223	0.1205	0.022	al, nsx, *sh*
OGLE-SMC-CEP-1049	1.204 2213(6)	0.736 700(9)	0.6118	0.1459	0.028	nsx, nsO
OGLE-SMC-CEP-1053	1.277 9760(9)	0.778 04(1)	0.6088	0.1460	0.027	
OGLE-SMC-CEP-1059	1.270 0610(7)	0.776 23(1)	0.6112	0.1570	0.023	nsO
OGLE-SMC-CEP-1119	1.659 938(2)	1.039 18(2)	0.6260	0.1327	0.032	sh, nsO, nsx, cf
OGLE-SMC-CEP-1127	1.638 464(2)	1.027 25(4)	0.6270	0.1315	0.023	sh, nsx, ap
OGLE-SMC-CEP-1138	1.492 0903(9)	0.913 13(2)	0.6120	0.1420	0.021	nsO, nsx
OGLE-SMC-CEP-1185	1.192 7515(9)	0.726 60(1)	0.6092	0.1644	0.026	
OGLE-SMC-CEP-1248	1.166 2128(5)	0.709 43(1)	0.6083	0.1559	0.019	
OGLE-SMC-CEP-1294	1.336 9590(8)	0.820 15(1)	0.6134	0.1443	0.022	ap
OGLE-SMC-CEP-1317	1.284 214(1)	0.780 28(1)	0.6076	0.1042	0.037	nsO
OGLE-SMC-CEP-1366	2.128 286(4)	1.324 63(5)	0.6224	0.0912	0.037	sh, nsO
OGLE-SMC-CEP-1482	1.339 5479(8)	0.814 39(1)	0.6080	0.1004	0.023	nsO, ap
OGLE-SMC-CEP-1496	1.334 207(1)	0.811 09(1)	0.6079	0.1444	0.032	cf, nsx
OGLE-SMC-CEP-1516	1.951 989(5)	1.219 60(6)	0.6248	0.0543	0.036	*sh*, ap, nsx
OGLE-SMC-CEP-1583	3.808 44(1)	2.4164(1)	0.6345	0.0929	0.033	nsx
OGLE-SMC-CEP-1710	2.115 741(1)	1.315 34(2)	0.6217	0.1237	0.025	sh, nsx, nsO
OGLE-SMC-CEP-1771	2.720 656(3)	1.738 77(5)	0.6391	0.0963	0.023	nsx, *sh*
OGLE-SMC-CEP-1773	2.048 935(2)	1.280 38(3)	0.6249	0.1102	0.023	sh, nsO, nsx
OGLE-SMC-CEP-1783	1.087 583(1)	0.669 32(1)	0.6154	0.1418	0.032	ap, nsx
OGLE-SMC-CEP-1802	2.608 860(3)	1.622 83(5)	0.6220	0.1043	0.024	nsx
	2.608 860(3)	1.667 77(7)	0.6393	0.1043	0.019	
OGLE-SMC-CEP-1856	1.898 340(1)	1.18132(1)	0.6223	0.1320	0.035	cf, sh, nsx
OGLE-SMC-CEP-1870	3.938 740(6)	2.49426(8)	0.6333	0.0980	0.027	nsO, cf, sh, nsx
OGLE-SMC-CEP-1882	1.296 622(1)	0.794 54(1)	0.6128	0.1089	0.029	tdp, nsO, nsx
OGLE-SMC-CEP-1975	1.907 327(2)	1.189 31(4)	0.6235	0.1477	0.019	sh
OGLE-SMC-CEP-1976	1.264 3772(8)	0.767 72(1)	0.6072	0.1421	0.028	nsO, nsx, tdp
OGLE-SMC-CEP-2009	1.962 690(2)	1.217 87(2)	0.6205	0.1118	0.032	nsx
OGLE-SMC-CEP-2033	1.408 7293(8)	0.858 69(1)	0.6095	0.1430	0.023	nsx, nsO
OGLE-SMC-CEP-2047	1.243 6705(7)	0.755 72(1)	0.6076	0.1480	0.027	nsx
OGLE-SMC-CEP-2116	1.488 366(2)	0.903 31(3)	0.6069	0.1394	0.025	nsx, nsO
OGLE-SMC-CEP-2126	1.371 930(1)	0.833 87(2)	0.6078	0.1530	0.039	al
OGLE-SMC-CEP-2131	2.602 695(3)	1.604 03(5)	0.6163	0.1363	0.015	al, nsO
OGLE-SMC-CEP-2178	2.476 222(4)	1.489 24(4)	0.6014	0.1114	0.031	nsx
	2.476 222(4)	1.534 94(6)	0.6199	0.1114	0.025	sh

Table A1 – *continued*

Star	P_{1O} (d)	P_x (d)	P_x/P_{1O}	A_{1O}	A_x/A_{1O}	Remarks
OGLE-SMC-CEP-2227	2.075033(1)	1.28790(3)	0.6207	0.1289	0.019	al, sh, nsx
OGLE-SMC-CEP-2253	3.460 665(5)	2.199 75(9)	0.6356	0.1011	0.023	*sh*, nsx, cf
OGLE-SMC-CEP-2285	2.020 254(3)	1.260 65(3)	0.6240	0.0864	0.038	nsO, tdp, sh, nsx
OGLE-SMC-CEP-2299	1.201 553(2)	0.730 48(2)	0.6079	0.1535	0.047	
OGLE-SMC-CEP-2374	1.078 9226(7)	0.657 98(1)	0.6099	0.1751	0.024	
OGLE-SMC-CEP-2433	2.389 605(2)	1.531 45(4)	0.6409	0.1160	0.028	*sh*, nsx
OGLE-SMC-CEP-2440	1.830 655(2)	1.143 10(3)	0.6244	0.1452	0.026	nsx, ap
OGLE-SMC-CEP-2497	1.184 7874(5)	0.724 76(1)	0.6117	0.1488	0.018	al, nsO, nsx
OGLE-SMC-CEP-2499	1.781 123(1)	1.113 33(2)	0.6251	0.1369	0.017	cf, nsO, nsx
OGLE-SMC-CEP-2501	1.258 3171(9)	0.764 52(1)	0.6076	0.1629	0.032	cf
OGLE-SMC-CEP-2528	1.460 9104(8)	0.885 43(2)	0.6061	0.1417	0.016	tdp, nsO
OGLE-SMC-CEP-2536	2.368 486(2)	1.513 26(6)	0.6389	0.1333	0.012	nsO, tdp, ? (S/N = 3.90)
OGLE-SMC-CEP-2567	2.260 065(5)	1.402 79(5)	0.6207	0.0983	0.041	sh, nsx
OGLE-SMC-CEP-2593	1.237 1639(9)	0.751 89(2)	0.6078	0.1568	0.021	
OGLE-SMC-CEP-2594	2.081 922(4)	1.295 30(3)	0.6222	0.1238	0.034	sh, cf, nsx
OGLE-SMC-CEP-2595	1.264 9697(6)	0.767 75(1)	0.6069	0.1475	0.024	nsx
OGLE-SMC-CEP-2597	2.572 680(3)	1.641 69(5)	0.6381	0.1149	0.025	nsx
OGLE-SMC-CEP-2627	2.074 554(2)	1.288 70(3)	0.6212	0.1194	0.032	al, nsx, *sh*
	2.074 554(2)	1.342 70(4)	0.6472	0.1194	0.023	
OGLE-SMC-CEP-2628	1.746 435(1)	1.087 73(2)	0.6228	0.1309	0.022	nsO, tdp, *sh*, nsx
OGLE-SMC-CEP-2681	2.076 572(2)	1.293 20(2)	0.6228	0.1197	0.039	sh, nsx
	2.076 572(2)	1.337 20(4)	0.6439	0.1197	0.024	
OGLE-SMC-CEP-2686	1.285 6603(7)	0.785 072(7)	0.6106	0.1504	0.032	nsO, cf
OGLE-SMC-CEP-2805	2.294 958(4)	1.418 12(4)	0.6179	0.1200	0.030	sh, cf
OGLE-SMC-CEP-2813	2.269 260(2)	1.407 83(2)	0.6204	0.1164	0.025	sh, cf, nsx
OGLE-SMC-CEP-2860	1.472 5949(7)	0.900 13(1)	0.6113	0.1455	0.019	al, nsO, nsx
OGLE-SMC-CEP-2866	0.880 405(1)	0.541 328(6)	0.6149	0.1652	0.027	nsO, tdp
OGLE-SMC-CEP-2883	2.675 263(5)	1.716 00(8)	0.6414	0.0977	0.024	cf
OGLE-SMC-CEP-2910	2.505 797(4)	1.604 40(8)	0.6403	0.1208	0.021	nsx
OGLE-SMC-CEP-2941	2.951 978(3)	1.876 80(7)	0.6358	0.1216	0.016	nsO, nsx, ap
OGLE-SMC-CEP-2958	1.293 953(1)	0.789 23(2)	0.6099	0.1404	0.018	
OGLE-SMC-CEP-2987	2.432 181(5)	1.517 20(6)	0.6238	0.1146	0.027	nsO, nsx
OGLE-SMC-CEP-3033	2.710 326(5)	1.726 10(8)	0.6369	0.1090	0.024	
OGLE-SMC-CEP-3040	2.493 781(3)	1.594 39(4)	0.6393	0.1198	0.021	nsO, *sh*, cf
	2.493 781(3)	1.496 04(5)	0.5999	0.1198	0.017	
OGLE-SMC-CEP-3094	2.565 406(3)	1.633 08(4)	0.6366	0.0999	0.025	nsx
OGLE-SMC-CEP-3098	1.366 169(1)	0.832 58(2)	0.6094	0.1582	0.021	al, nsx
	1.366 169(1)	0.857 52(3)	0.6277	0.1582	0.018	
OGLE-SMC-CEP-3143	1.062 0663(6)	0.650 56(1)	0.6125	0.1872	0.017	
OGLE-SMC-CEP-3172	1.662 515(1)	1.037 77(2)	0.6242	0.1271	0.025	sh, nsx, nsO
OGLE-SMC-CEP-3210	1.196 9483(5)	0.729 788(9)	0.6097	0.1546	0.025	nsO
OGLE-SMC-CEP-3239	1.796 954(2)	1.117 60(3)	0.6219	0.1446	0.031	nsx, *sh*
OGLE-SMC-CEP-3249	1.262 314(2)	0.767 82(2)	0.6083	0.1154	0.027	nsO, tdp
OGLE-SMC-CEP-3292	2.501 456(2)	1.548 22(4)	0.6189	0.1283	0.020	nsO, cf, ap, *sh*
OGLE-SMC-CEP-3298	2.680 077(2)	1.712 42(5)	0.6389	0.1194	0.019	nsO, sh, cf, nsx
OGLE-SMC-CEP-3303	1.841 813(3)	1.147 80(4)	0.6232	0.1115	0.026	nsO, nsx, tdp, ap
OGLE-SMC-CEP-3310	1.520 1938(9)	0.921 63(2)	0.6063	0.1035	0.017	? (S/N = 3.79), nsO
OGLE-SMC-CEP-3312	2.117 703(2)	1.320 09(3)	0.6234	0.1227	0.024	sh, nsx
OGLE-SMC-CEP-3317	2.000 277(6)	1.248 93(5)	0.6244	0.1217	0.024	sh, nsO, nsx
OGLE-SMC-CEP-3319	3.088 226(7)	1.9626(1)	0.6355	0.0972	0.025	al, nsx
OGLE-SMC-CEP-3343	1.831 819(2)	1.144 84(2)	0.6250	0.1208	0.038	sh, cf, nsx
OGLE-SMC-CEP-3349	1.922 025(3)	1.203 43(3)	0.6261	0.1031	0.029	sh, al, nsx, cf
OGLE-SMC-CEP-3479	1.164 4782(8)	0.711 81(1)	0.6113	0.1550	0.028	ap
OGLE-SMC-CEP-3493	1.704 786(1)	1.034 61(2)	0.6069	0.1492	0.020	cf
OGLE-SMC-CEP-3541	1.329 9750(6)	0.809 77(1)	0.6089	0.1558	0.018	nsO, nsx
OGLE-SMC-CEP-3576	1.585 9739(8)	0.962 88(1)	0.6071	0.1473	0.018	nsx, cf
OGLE-SMC-CEP-3590	2.007 673(1)	1.252 95(2)	0.6241	0.1389	0.020	*sh*, cf, nsx
OGLE-SMC-CEP-3624	1.461 0331(7)	0.890 74(2)	0.6097	0.1541	0.014	? (S/N = 3.58)
OGLE-SMC-CEP-3668	2.738 933(3)	1.747 19(4)	0.6379	0.1203	0.020	nsO, cf, nsx
OGLE-SMC-CEP-3789	1.424 0538(7)	0.869 23(1)	0.6104	0.1441	0.020	
OGLE-SMC-CEP-3903	0.954 6276(6)	0.585 94(1)	0.6138	0.1822	0.018	? (S/N = 3.77)
OGLE-SMC-CEP-3913	3.053 017(4)	1.937 93(7)	0.6348	0.1166	0.018	al
OGLE-SMC-CEP-3944	2.162 091(2)	1.347 39(3)	0.6232	0.0989	0.028	sh, nsx, nsO
OGLE-SMC-CEP-3977	1.542 764(3)	0.967 93(3)	0.6274	0.1187	0.044	al
OGLE-SMC-CEP-3987	3.368 937(9)	2.1393(1)	0.6350	0.1025	0.038	al, *sh*, nsO, nsx

Table A1 – *continued*

Star	P_{1O} (d)	P_x (d)	P_x/P_{1O}	A_{1O}	A_x/A_{1O}	Remarks
OGLE-SMC-CEP-4011	1.814 599(2)	1.135 16(3)	0.6256	0.1368	0.025	sh, nsx, cf
OGLE-SMC-CEP-4046	2.248 845(4)	1.398 08(4)	0.6217	0.1210	0.036	sh, nsx, cf
OGLE-SMC-CEP-4061	2.573 926(3)	1.647 45(6)	0.6401	0.1125	0.018	nsx, nsO
OGLE-SMC-CEP-4068	2.010 614(2)	1.247 62(2)	0.6205	0.1231	0.028	sh, nsO, nsx
OGLE-SMC-CEP-4157	1.256 266(1)	0.761 87(3)	0.6065	0.1485	0.021	? (S/N = 3.34)
OGLE-SMC-CEP-4188	1.520 138(1)	0.924 75(2)	0.6083	0.1482	0.021	ap
OGLE-SMC-CEP-4205	1.944 865(3)	1.212 86(2)	0.6236	0.1208	0.049	sh, nsx, cf
OGLE-SMC-CEP-4232	1.721 685(2)	1.074 01(5)	0.6238	0.1536	0.015	? (S/N = 3.76)
OGLE-SMC-CEP-4250	1.466 489(1)	0.894 68(3)	0.6101	0.1502	0.021	
OGLE-SMC-CEP-4255	2.091 244(5)	1.306 21(5)	0.6246	0.0988	0.038	sh, al, nsx
OGLE-SMC-CEP-4262	2.093 166(6)	1.303 18(5)	0.6226	0.0885	0.049	sh, nsx
OGLE-SMC-CEP-4303	1.167 9163(9)	0.713 44(1)	0.6109	0.1487	0.030	al, nsO, nsx
OGLE-SMC-CEP-4316	1.295 785(1)	0.787 25(1)	0.6076	0.1686	0.029	
OGLE-SMC-CEP-4378	2.673 50(2)	1.7078(1)	0.6388	0.1035	0.030	nsO, tdp, al
OGLE-SMC-CEP-4388	2.034 294(5)	1.266 59(5)	0.6226	0.1024	0.044	sh
OGLE-SMC-CEP-4394	1.095 018(1)	0.671 56(1)	0.6133	0.1309	0.032	nsO
OGLE-SMC-CEP-4395	2.869 590(7)	1.8288(1)	0.6373	0.1110	0.030	*sh*, nsx
OGLE-SMC-CEP-4462	2.136 558(4)	1.324 84(6)	0.6201	0.1031	0.029	sh, nsx
OGLE-SMC-CEP-4587	1.141 6708(7)	0.698 56(1)	0.6119	0.1761	0.024	
OGLE-SMC-CEP-4627	3.173 04(2)	1.957 69(5)	0.6170	0.0735	0.105	cf, ap

OGLE-SMC-CEP-1127 – the difference for this star is a result of long-term trend, likely not removed by S10. Its one-day alias falls at $P/P_{1O} \approx 0.6084$ and was interpreted as additional variability in S10. The trend is well visible in the residual data. After removing the trend with third-order polynomial, the one-day alias also disappears, but another signal at $P_x/P_{1O} \approx 0.6270$ is present, which we interpret as due to additional variability.

OGLE-SMC-CEP-2131 – the difference for this star is a result of strong non-stationarity of the first overtone. One-day alias (at $P/P_{1O} \approx 0.6215$) of the strong, residual peak at the frequency of first overtone was likely interpreted as additional variability by S10. After time-dependent pre-whitening, the ambiguous signal disappears, but we detect another significant peak nearby, at $P_x/P_{1O} \approx 0.6163$, and interpret as due to additional variability.

OGLE-SMC-CEP-3094 – after pre-whitening with v_{1O} and its harmonics (and detrending) the strongest peak is present at $P_x/P_{1O} = 0.6366$, as given in Table 1. Its daily alias falls very close to v_{1O} (resolved) and likely was pre-whitened by S10 first. Then, the highest peak is found at $P_x/P_{1O} \approx 0.6327$ as is reported in S10. Both solutions are likely.

OGLE-SMC-CEP-3098 – after pre-whitening with v_{1O} and its harmonics (and detrending), the strongest peak in the $P/P_{1O} \in (0.6, 0.65)$ range is detected at $P_x/P_{1O} \approx 0.6094$ as reported in Table 1. Its daily alias is higher however, it falls at $P/P_{1O} \approx 0.913$ and can be interpreted as other periodicity. In S10, this peak was likely pre-whitened first. Then, the highest peak in the frequency range of interest appears at $P_x/P_{1O} \approx 0.6101$ as reported in S10. Both solutions are likely.

OGLE-SMC-CEP-3349 – after pre-whitening with v_{1O} and its harmonics (and detrending), the highest peak in the frequency range of interest appears at $P_x/P_{1O} \approx 0.6261$, as reported in Table 1. Its daily alias is higher however. There are two lower peaks around; one of them at $P_x/P_{1O} \approx 0.6217$ was reported in S10 (interestingly its daily alias is also higher).

OGLE-SMC-CEP-4255 – after pre-whitening with v_{1O} and its harmonics (and detrending), the strongest peak in the $P/P_{1O} \in (0.6, 0.65)$ range is detected at $P_x/P_{1O} \approx 0.6246$ (S/N = 5.16) as given in Table 1. Its daily alias is higher however, it falls at $P_{1O}/P = 0.496$ (S/N = 5.29). In S10, this peak was likely pre-whitened first. Then, the highest peak in the frequency range of interest appears at $P_x/P_{1O} \approx 0.6252$ as reported in S10. Both solutions are likely.

In eight stars, the highest peak in the frequency range of interest corresponds to P_x/P_{1O} falling well within one of the three sequences visible in Fig. 1 (stars marked with triangles), but the S/N is below 4.0 (it is reported in the last column of Table 1; these stars also have '?' in remarks column). Frequency spectra for these stars are plotted in Fig. B1. Likely the additional variability is present in these stars but its amplitude is small as compared to the noise level.

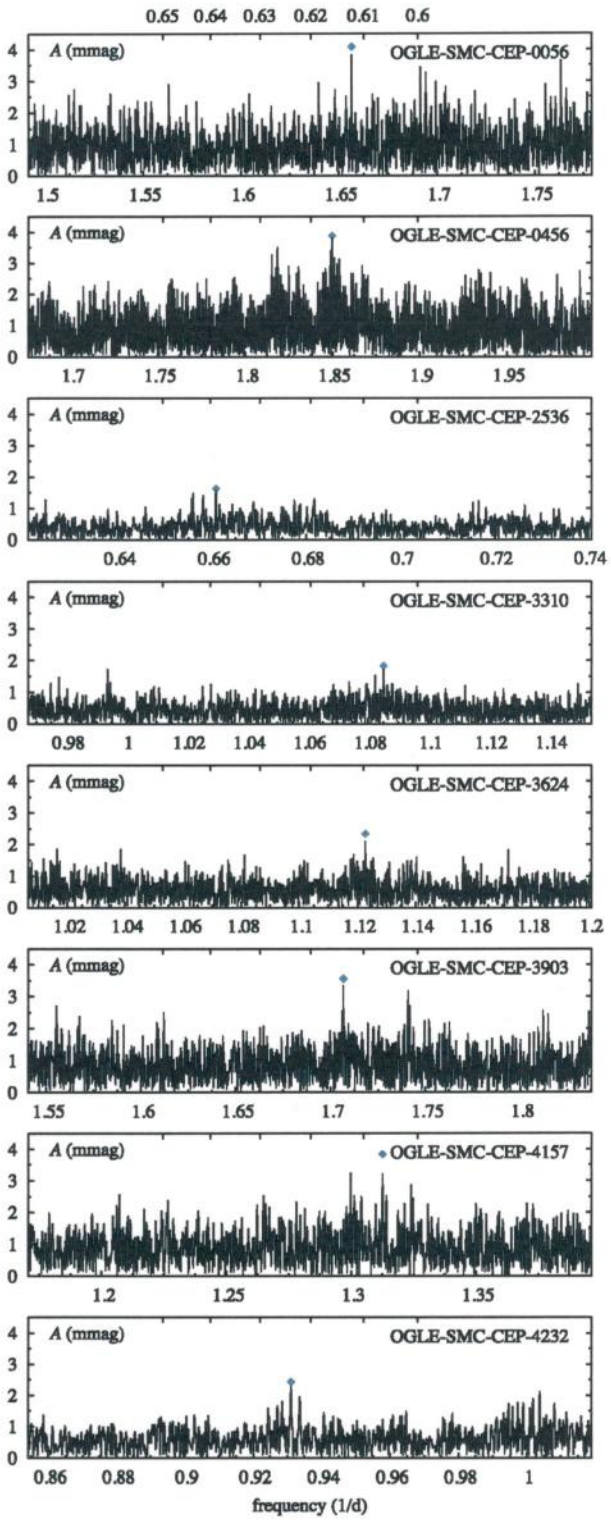

Figure B1. Frequency spectra for eight stars in which detection of the additional variability is weak, with $3.0 < S/N < 4.0$. Diamond marks the location of the peak and is placed exactly at $S/N = 4.0$. Ticks at the top axis of each panel correspond to P/P_{1O} scale, explicitly given at the top of the Figure.

This paper has been typeset from a TEX/LATEX file prepared by the author.